Effects of high magnetic fields on the behavior of feeble magnetic fluids

WANG Yan
Doctoral Program in Materials Science and Engineering

Submitted to the Graduate School of
Pure and Applied Sciences
in Partial Fulfillment of the Requirements
for the Degree of Doctor of Philosophy in
Engineering

at the
University of Tsukuba

To my beloved parents and wife

Thesis abstract

The fluid flow plays a significant role in many material processes to decide the quality and performance of products. The control of fluid flow has been a crucial issue to improve materials qualities. Magnetic fields are regarded as an attractive means to control the fluid behavior due to the dynamical effects on materials can be induced without direct contact. This feature, for example, enables us the contamination-free processing. Magnetic control of fluid flow is based on “the magnetic force” and “the Lorentz force” and has been actually applied in many industrial processes, especially for the control of convection in molten metals. Numbers of efforts have been devoted to understand the effects of magnetic field on the flow structure and stability of feeble magnetic fluid. However, there are still some phenomena not enough understood remaining, such as the fluid behavior in the solid-liquid coexisting system or high temperature processing. Particularly, owing to the high temperatures and low light transparencies of liquid metals, the majority of investigations are based on computer simulations, and there are a limited number of evidences experimentally obtained on the behaviors of conductive melts in magnetic fields.

The objective of this thesis is to improve the magnetic control of fluid flow by experimental observation of fluid behavior under high magnetic fields. For flow of non-conductive fluid, the effect of magnetic force was considered. An *in-situ* optical observation system was developed based on Schlieren technique to visualize the fluid motion in non-conductive transparent solution under high magnetic fields. For flow of conductive fluid, both the effects of Lorentz force and magnetic force were considered. The electrolyte aqueous solutions combined with a superconducting magnet were used as substitution of liquid metals in industrial electromagnets since flow conditions thereby were regarded as similar. Effects of magnetic fields on the thermal convection in such conductive aqueous solutions at ambient temperatures were then studied through heat transport measurements combined with shadowgraph technique-based visualization. The following are the accomplishments of this thesis.

Effects of high magnetic field on non-conductive fluid flow

The *in-situ* optical observation system utilizable in high magnetic fields was developed based on Schlieren technique. The fluid motions of optically transparent solution were successfully observed even in high magnetic field owing to the difference of the reflective index that depends on the concentration of solution. It was observed that the direction of diamagnetic non-conducting fluid flow was changed under spatially varied magnetic field. This phenomenon was understood qualitatively by considering the magnetic force acting on the high concentration solution and the surrounding solution.

Effects of high magnetic field on conductive fluid flow

Under the magnetic fields up to 12.0 T, the thermal convection in conductive solution was suppressed. The magnitude of this suppression effect depends on the applied magnetic field and the concentration of sample solutions. Through the comparison of magnetic field effects on diamagnetic and paramagnetic conductive fluids, it was found that the magnitude of this suppression effect depends on the electrical conductivity of sample fluids regardless of their magnetism. This suppression of the thermal convection of conductive fluids under the magnetic field was therefore experimentally confirmed as the effect of the Lorentz force.

The magnetic induction and damping of the thermal convection of the conductive fluid were experimentally demonstrated. Furthermore, the contribution of the Lorentz force and magnetic force on the thermal convection of feeble magnetic conductive fluids was separately evaluated by changing the magnetic field environment. These results show that the effect of the Lorentz force and the magnetic force can be investigated individually by using electrolytes aqueous solution combined with a superconducting magnet.

Owing to these experimental observation, the understanding of feeble magnetic fluid behavior under high magnetic fields was deepened. Especially, this thesis shows that, it seems feasible to understand the behaviors of liquid metals by using electrolytes aqueous solution combined with a superconducting magnet since flow conditions thereby are regarded as similar to those for liquid metals in industrial electromagnets. Use of aqueous solutions enables us experiments under room temperature and also expected to bring spatial information about the convection in a fluid since they have optical transparency in many cases. Through the comparison of the obtained experimental evidence with the related numerical simulation results, the feeble magnetic fluid behavior under magnetic fields can be further understood and thus magnetic control processing can be promisingly optimized.

Acknowledgement

I would like to take this great opportunity to acknowledge all of the help that I have received along the way. Great thanks must go to my supervisor, Prof. Yoshio Sakka, for all the support that he has given me over the past three years, and for helping to make my Ph.D. studies both enjoyable and rewarding.

I would like to express my deepest gratitude to Dr. Noriyuki Hirota, for his effort, support and advice which played a key role to complete my PhD thesis. He has been in all regards the ideal mentor that giving me a great deal of independence while at the same time always being available to help. I am grateful to him for having been so much patient with my imperfection. These experiences have greatly enhanced my education and molded me into an independent researcher.

I also wish to thank the members of my Ph.D. committee, Prof. Yoshihiko Takeda, Prof. Tetsushi Taguchi and Prof. Hideto Yanagihara for their guidance, reviewing my thesis and proposing valuable suggestions.

My sincere thanks is also given to Dr. Hidehiko Okada for his comments that have always led to improvements in my study.

My thanks go to everyone in the materials processing unit of the National Institute for Materials Science, for all their help, support and every valuable comments during my study here.

I also address my personal gratitude to Mr. Chunhui Zhao who helped me a lot during my PhD course, both in study and life.

I am also thankful to Ms. Yuko Yamaguchi, Ms. Masako Tamiya and Ms. Yoko Watanabe for their continuous help in all kinds of matters during my staying in Japan.

I wish to express my sincere gratitude to Prof. Qiang Wang and Dr. Tie Liu in Northeastern University of China for all the help and support they have given me.

I would like to acknowledge the China Scholarship Council and the Ministry of Education of the P. R. China for their financial support during my Ph.D. period and otherwise.

Finally, I owe my deepest appreciation to my father, my mother, my wife and the rest of my family for the huge love and support they have provided me throughout my life.

Contents

Chapter 1

Introduction

- **Fluid flow in material processing**
- **Method of fluid flow control**
- **Dynamical effects of magnetic field**
- **Fluid behavior under high magnetic fields**

1.1 Fluid flow in material processing

The fluid flow appears everywhere not only in nature but also in our daily life. The control of fluid flow is often necessary to achieve specific outcomes in many scientific and industrial applications, for example material processing. In material preparation processes, the fluid flow influences many properties including heat transfer, mass transfer, segregation of inclusions, crystal growth, etc. [1-3]

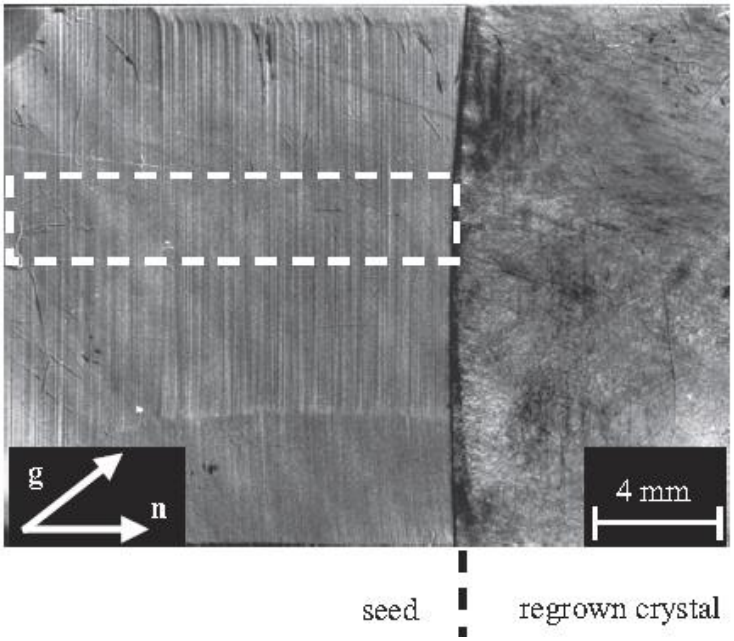

Figure 1.1 Structural features of the GaSb(Si) crystal grown by the Czochralski method (at the left) and partially regrown by the vertical Bridgman method (at the right).

During the crystal growth processing, it has been known that the unsteady thermogravity convection in the melt gives rise to growth rate oscillations and leads to the formation of growth striations (micro-inhomogeneities) in crystal. [4] As shown in figure 1.1, the GaSb(Si) single crystal was grown by Czochralski method (left-hand part). [5] Characteristic features of the seed at left – hand part in the figure are the microsegregation pattern, low dislocation density and the macroscopic inhomogeneity of the dopant distribution, caused by the facet effect and convection in the melt. Similar defections caused by convection also appear in the solidification processing, as shown in figure 1.2. [6] The freckle defect was caused by the natural convection appeared in the melt of Ni-based superalloy during single-crystal directional solidification process.

However, utilizing the feature of fluid flow in the melt, good effects can also be induced in material processing. As showed in figure 1.3, during the polyethylene solution crystallisation processing, only chain folded single crystal can be formed without induced flow in the solution. However, with an appropriate induced flow in the solution, crystal with a special structure, such as Shish kebab fibrous crystal, can be obtained. By controlling the flow condition in the solution, millions of polyethylene polymer chains can be ordered to form beautiful structures. [7]

Figure 1.2 The freckle defects in single-crystal Ni-based superalloy.

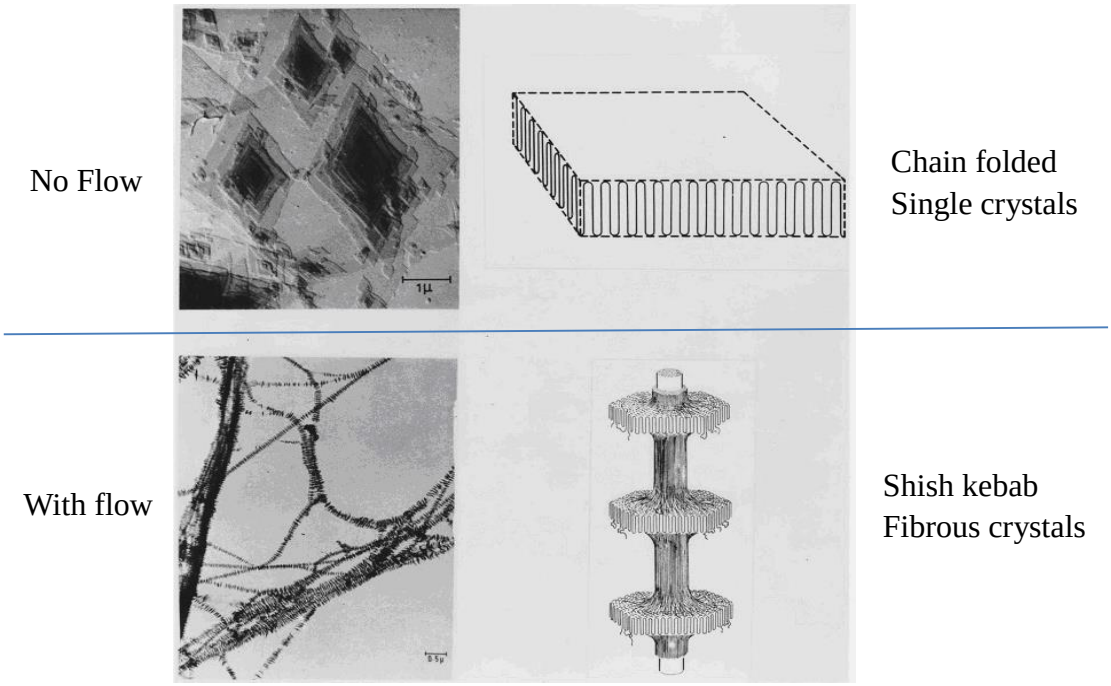

Figure 1.3 Structure of polyethylene polymer chains formed single crystal.

Furthermore, as shown in the figure 1.4, the grain structure of Al-7wt%Si alloy was significantly refined by electromagnetic stirring process. [8] The grain structure and the transition from a columnar to equiaxed dendritic growth of crystals were remarkably affected by the forced convection. The refinement of grain size will of course improve the quality of alloy, for example, better feeding to avoid shrinkage porosity, reduction of hot tearing, improvement of strength and fatigue life and so on.

As we can see from these examples, the fluid flow has significant impact on quality and performance of products in many material processing. The control of fluid flow has been one of the key technology to improve the quality of material.

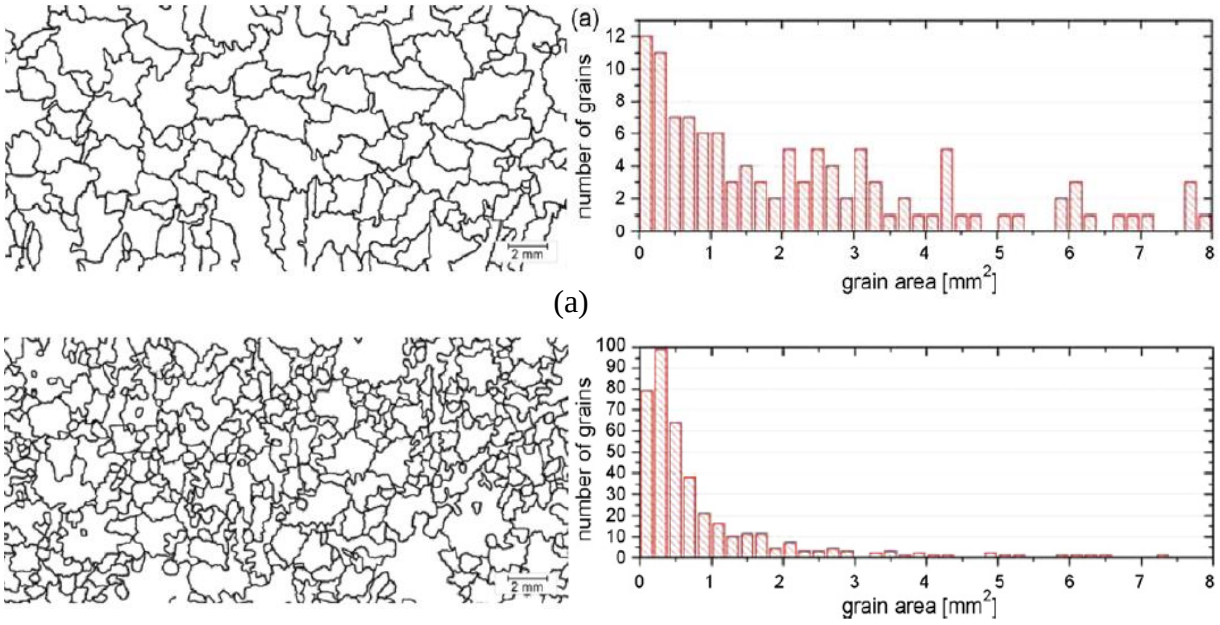

Figure 1.4 Grain structures of Al–7 wt.%Si alloys without stirring of melt (a) and with electromagnetic stirring of melt (b) during the solidification processing.

1.2 Method of fluid flow control

A lot of attempts have been presented by researchers to control the fluid behavior in the material processing, such as space-based microgravity, forced convection, centrifugation and application of magnetic field etc. Some examples and applications were described here.

1.2.1 Space-based microgravity

The natural convection in gravitational field is exist everywhere in the nature. The fluid motion is generated by buoyancy force due to density differences in the fluid. The heat transfer, mass transfer and other properties in a melt were significantly affected by natural convection in material processing such as the solidification processing and crystal growth processing. However, in the reduced gravity condition, the convective fluid motion driven by the buoyancy force can be effectively suppressed. In consequence, the space-based microgravity experiment was suggested by researchers and supported by institutions like the National Aeronautics and Space Administration (NASA) of United States of America. Many experimental investigations have been addressed to study the influence of microgravity environment on material processing in the space. [9-13] These works sufficiently proved that the buoyancy driven convection can be effectively damped in such Space-based microgravity environment.

For example, during the protein crystal growth processing, the diffusive field around a crystal will not be disturbed in space [9] and the depletion zone of protein and impurities around the growing crystal is supposed to be formed. Therefore, in the microgravity environment, the growth speed of

crystals may become decreased and the impurity uptake may be suppressed to result in highly ordered crystals. [10]

For the solidification processing of alloy, Billia et al. conducted experiments on the morphological stability of directionally solidified Pb-Ti samples in the gradient-heating facility during the Dl mission of NASA. [13] Due to the solute convection in the melt at the interface in concentrated alloys (25, 30 and 40 wt%Ti), the morphology of the cellular pattern was strongly influenced. For instance, the comparison between earth and space samples of the Pb-25 wt% Ti alloy shows that several convective-induced rolls were developed in the ground experiment and destroying the regularity of the cells, shown in figure 1.5. On earth, the shape of the cells is affected by four convective rolls. However, in space the cells are more regular and are coarser.

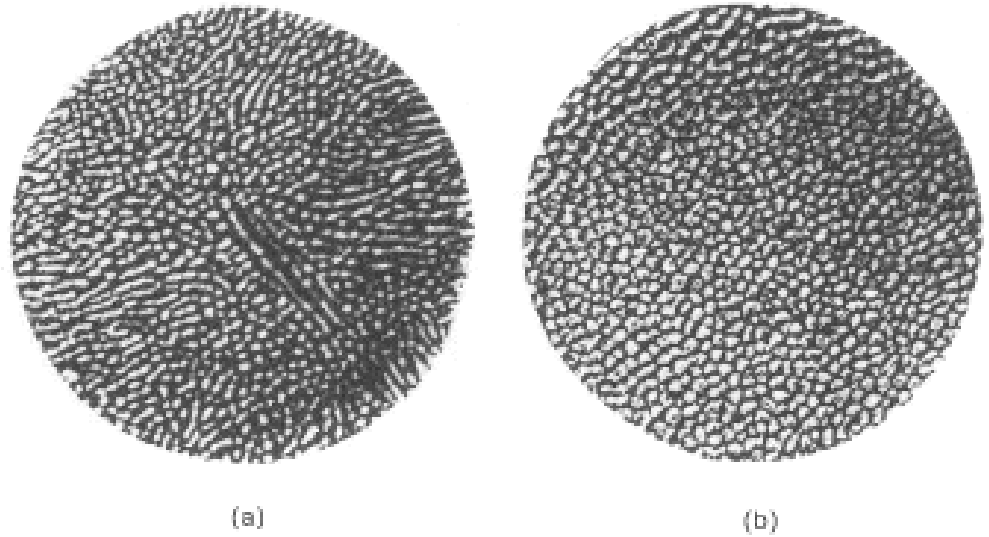

Figure 1.5. Comparison between corresponding cross sections of Pb-25 wt%Ti samples grown vertically (a) on earth and (b) in space.

Owing to the precious opportunities for space-based microgravity experiment provided by institutions like NASA, numbers of valuable achievements have been obtained. However, the experimental research in space is still costly and limited. Moreover, the convection in fluid cannot be enhanced or induced by microgravity environment.

1.2.2 Forced convection

To induce convection in a fluid, one of the most simple and direct way is the forced convection. By stirring the melt directly, using mould with special shape or crystal rotation etc., the fluid low can be easily induced in the melt, hence the quality of material will be affected.

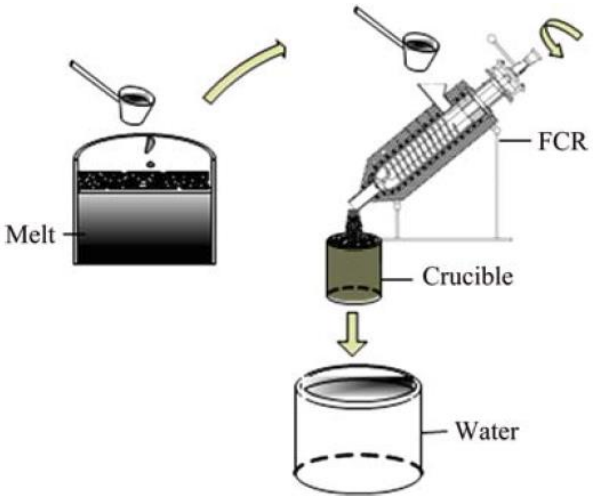

Figure 1.6 Schematic diagram of forced convection rheoforming process.

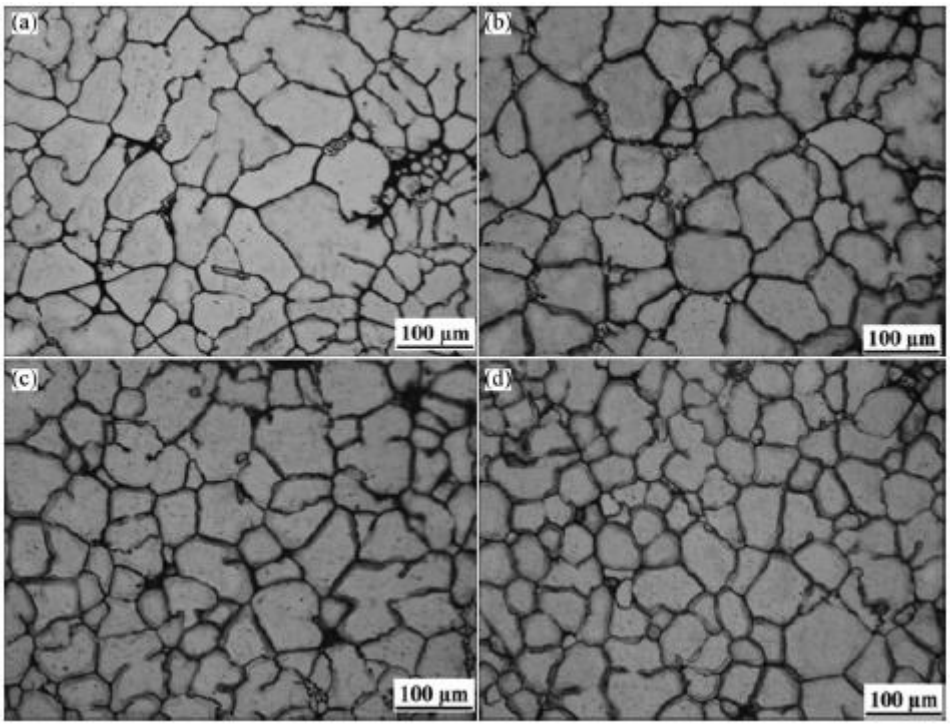

Figure 1.7 Optical micrographs of semisolid 7075 aluminum alloy in forced convection rheoforming process at different stirring speeds: (a) 100 r/min; (b) 200 r/min; (c) 300 r/min; (d) 400 r/min

For example, a forced convection rheoforming machine was designed for the preparation of light alloy semisolid slurry by Kang et al, as shown in figure 1.6 [14,15]. Owing to the rotation of churn-dasher, the fluid low can be induced easily and the stirring speed can be controlled. Taking 7075 aluminium alloy as experimental material, the microstructure characteristics and microstructure evolution of the alternative semisolid metal slurry at different stirring speeds were showed in figure 1.7. It can be seen that the semisolid microstructure of the 7075 Al alloy was dramatically affected by the induced flow.

However, to induce the forced convection, direct contact with the melt seems unavoidable and that means the contamination was much easier to be introduced.

1.2.3 Centrifugation

The utilization of a centrifuge, so-called centrifugal or high-gravity processing, is also considered as an effective method to modify the flow status in a melt. [16,17]

The way of using the centrifuge in crystal growth processing has always been in the free-swinging configuration, in which the sample is fixed at the end of a rotating arm. In such condition, the resultant acceleration is antiparallel to the axial thermal gradient, which is thus intuitively thermally stable. Therefore, the convection can be suppressed at a certain rotation rate, or the so-called magic-*g* level [17], where the Coriolis force balances the gravitational acceleration. Beyond the magic-*g* level, the centrifugal acceleration becomes important and the centrifugal thermal convection increases.

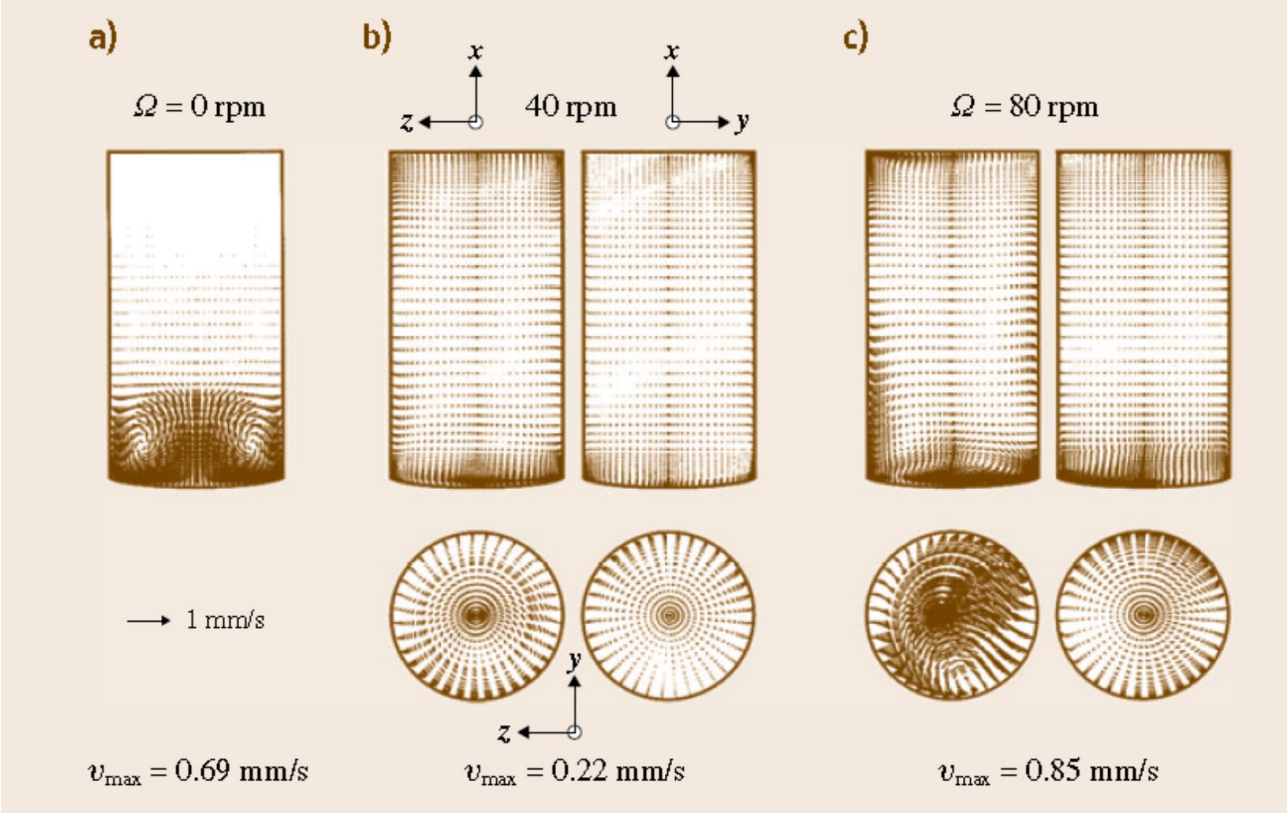

Figure 1.8 Effect of free-swing rotation on the flow fields for a gradient freeze growth of GaAs: (a) 0 rpm; (b) 40 rpm; (c) 80 rpm.

Figure 1.8 shows simulated flow patterns of germanium during Bridgman growth in a free-swing centrifuge at different rotation speed [16,18]. For 0 rpm (Figure 1.8 a) the flow is axisymmetric and the structure is typical for the vertical Bridgman configuration, with a concave interface; the heating temperature profile is linear. At 40 rpm the flow near the growth interface is significantly damped by the Coriolis force and the flow structure is also changed dramatically. Although the averaged resultant gravity direction is still antiparallel to the growth axis, the centrifugal acceleration and the Coriolis

force in the melt are asymmetric, leading to the 3-D flow. Owing to the non-uniform forces, the global convection increases slightly away from the interface. When the rotation speed is further increased to 80 rpm, as can be observed from the larger velocity vectors, the centrifugal force becomes dominant and the convection increases. The flows in the x–y plane are also shown, but are in general featureless except for the flow near the growth interface.

A number of efforts have been devoted to study the centrifugal field effect on convection in the melt during crystal growth. However, the application of centrifuge on fluid control is still limited and the increasing contact between melt and wall of container seems make contamination can be introduced easier.

1.2.4 Application of magnetic field

Compared with flow control methods which need to contact with the matter, a clear advantage to the use of magnetic field is that dynamical effects on materials can be induced without direct contact. This feature, for example, enables us the contamination-free processing. Therefore, numbers of researches on magnetically fluid flow control have been devoted [19-22] and this technique has been widely used in many industrial processes.

For example, for the silicon single crystals preparation processing, the magnetic Czochralski method has been widely used. When a static magnetic field was applied, the flow state in the melt become stable and the concentration of oxygen, which is one of the most harmful contamination for single crystal silicon, was dramatically decreased, as showed in figure 1.9 (b). [23] The quality of single crystal silicon was therefore improved.

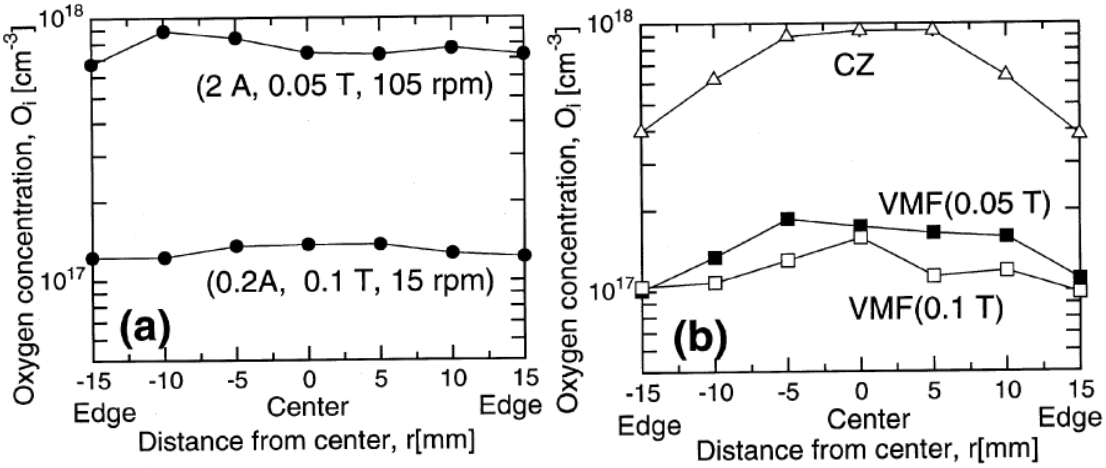

Figure 1.9 Oxygen concentration distribution in the radial direction in the crystals. (a) electromagnetic Czochralski crystals grown at higher rotation rate (105 rpm, I = 2.0 A, B = 0.05 T) and lower rotation rate (15 rpm, I = 0.2A, B = 0.1 T), (b) Czochralski (CZ) and vertical magnetic field (VMF) (0.05 T, 0.1 T) crystals.

Furthermore, the application of magnetic field was also used in steelmaking, casting and soildification processing. For example, Yasuda et al. [22] has summaried the trends of the application technology of magnetohydrodynamics (MHD) used or under development in steelmaking process in

terms of the functions of MHD, such as heating, stirring, braking, shaping and sensing, as shown in table 1.1.

Table 1.1 Application examples of MHD to steelmaking process.

Principle	Function	Field	Applications for steelmaking
Lorentz force	Shape control	AC	Electromagnetic Casting, Cold Crucible
	Flow Promotion	AC	Electromagnetic Stirring, Electromagnetic Pump
	Flow Suppression	AC/DC	Wave Suppression, Electromagnetic Brake
	Levitation	AC	Electromagnetic Casting, Cold Crucible, Convectional Levitation, Edge Containment
	Solidification Structure Control	AC	Electromagnetic Stirring, Pulse Current Imposition
	Separation	AC/DC	Inclusion Removal
Joule Heating	Heating	AC	Induction Heater
		DC	Plasma Heater
Lenz's Law	Detection	AC	Level Sensor, Velocimetry, Slag Flowout Detection
Magnetic force	Separation	DC	Particle Separator
	Precipitation Control	DC	Tramp Element Control

(AC : Alternative Current, DC : Direct Current)

As described above, the application of magnetic field has been used or developed in many industry precesses to control the flow in melt, and promisingly improved the quality of material. However, some limitations of the magnetic control are still remained, and some expamples are listed as below.

1) Control of micro flow. The macroscopic fluid motion in a melt has been proved that can be well controlled by application of magnetic field. However, the micro flow, such as the plume flow near the surface of dendrite, is still difficult to be accurately controlled at present.

2) Magnitude of fluid control. The intensity of the applied magnetic field in the practical industry environment is normally limited as below 1 T since the generation of magnetic field needs considerable electric energy. Therefore, the magnitude of the magnetically induced dynamical force acted on fluid flow is also limited.

3) Fluid of low electric conductivity. At present, the magentic control of fluid flow in the industry processing is mainly focused on the conductive fluid such as melt metal and based on the induced Lorentz force. This induced Lorentz force strongly depends on the electrical conductivity of fluid. Therefore, for the fluid with a low electric conductivity, the intensity of induced Lorentz force is also weak.

Owing to these limitations, the magnetic control of fluid flow in the meterial processing still needs to be improved.

1.3 Dynamical effects of magnetic field on fluid flow

To control the fluid behavior, dynamical effects induced by magnetic field are mainly based on "the magnetic force" and "the Lorentz force". These two forces are briefly introduced here to help understanding of the fluid motion in magnetic field.

1.3.1 Lorentz force

The Lorentz force arises from the interaction of a moving electric charge and a magnetic field. When an electric charged particle moves perpendicular to the magnetic field, it receives a Lorentz force F_L, [24]

$$F_L = J \times B = qv \times B \tag{1.1}$$

Here J is the electric current density, B is the magnetic flux density, q is the electric charge of particle and v is the velocity of particle.

The characteristics of Lorentz force are summarized in Table 1.2 [25] The Lorentz force is proportional to the B. It induces a torque on the electrically charged particle in the plane perpendicular to B and induces rotational motion. The direction of the torque is reversed when the direction of B is reversed.

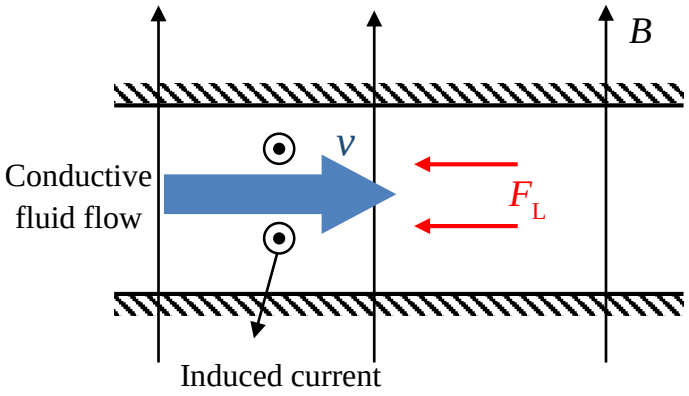

Figure 1.10 Schematic of Lorentz force acted on conductive fluid flow in a static magnetic field.

For the conductive fluid, the electric current induced in the fluid as a result of its motion modifies the field. At the same time, the flow in the magnetic field produces a mechanical force which modify the motion. Details and explanations were showed in figure 1.10, when the conductive fluid flow moves perpendicular to applied magnetic field, the electric current was induced due to the interaction between velocity field and the magnetic field. The direction was pointed out of paper. At the same time, the Lorentz force was produced due to the interaction between induced current and magnetic field. With a static magnetic field, the direction of the Lorentz force will always be opposite to the velocity direction of conductive fluid which moved perpendicular to the magnetic field. It is the principle for magnetic field damping of liquid metal convection. [26]

Table 1.2 Comparison of magnetic force and Lorentz force

	Magnetic force	Lorentz force
Interacting physical quantity	Magnetic susceptibility	Electric charge
Type of MF*	Nonhomogeneous	Homogeneous
MF dependence	Quadratic (B^2)	Linear (B)
Direction of force	Parallel or anti-parallel to MF Linear	Perpendicular to MF
Inversion of MF	Invariant	Inverted

* MF : magnetic field

In solution, ions and charged particles cannot move alone due to collision with the solvent and other solutes. As a result, the Lorentz force induces convection of the solution with an imposed or induced electric field. This mechanism is call the magnetohydrodynamics (MHD) mechanism. It is important in not only electrochemical reactions where electric current moves in solution but also in processes in solution where ions move to a specific reaction zone such as the solid liquid interface. The MHD effect was first investigated in macroscopic system of electrolysis [27], and more recently for microscopic system in relation to the morphology of electrochemical products. [28]

The Lorentz force has been widely used for induction or suppression of convection in the practical industry, for example the previous mentioned single crystal silicon preparation processing and steel making process.

1.3.2 Magnetic force

Magnetic force arises from the interaction of the magnetism of a material and a magnetic field. When a material is positioned in a gradient magnetic field, the body is acted on by a magnetic force, as expressed below: [29]

$$F_m = -\frac{\partial E_m}{\partial z} = \frac{\chi_v}{\mu_0} B \frac{\partial B}{\partial z} \tag{1.2}$$

Where E_m is the isotropic magnetic energy, χ_v is the volume magnetic susceptibility and μ_0 is permeability of vacuum.

Characteristics of magnetic force are also listed in Table 1.2. The magnetic force depends on the magnetic susceptibility of material, the density of magnetic flux and the magnetic field gradient. The force is dependent on B^2. It is linear and parallel or anti-parallel to that of $\partial B/\partial z$. Materials can be either repelled (diamagnetic material, $\chi_v < 0$) or attracted (paramagnetic material, $\chi_v > 0$) based on their magnetic susceptibility. The direction of the force is invariant when the magnetic field direction is changed to the opposite one. One can differentiate the effects of the magnetic force and

the Lorentz force using Table 1.2.

As a mechanical effect of magnetic fields, the magnetic force is very important. For example, the aqueous solution of paramagnetic ions in water can be moved simply by using a conventional permanent magnet (0.2-0.3 T). [30] It is also possible to separate paramagnetic ions [31] and paramagnetic particles. [32]

This force is quite weak for usual diamagnetic substances in ordinary fields due to their feeble magnetic property. However, recently, the product $B(\partial B/\partial z)$ can be enhanced with the aid of high field magnets, such as super-conducting magnet. Consequently, some diamagnetic materials, such as water and organic compounds, can be also levitated in air by applied magnetic fields which range up to 20 T or more. [33] Therefore new functional materials can be synthesized under microgravity in laboratories on Earth, not in space. [34]

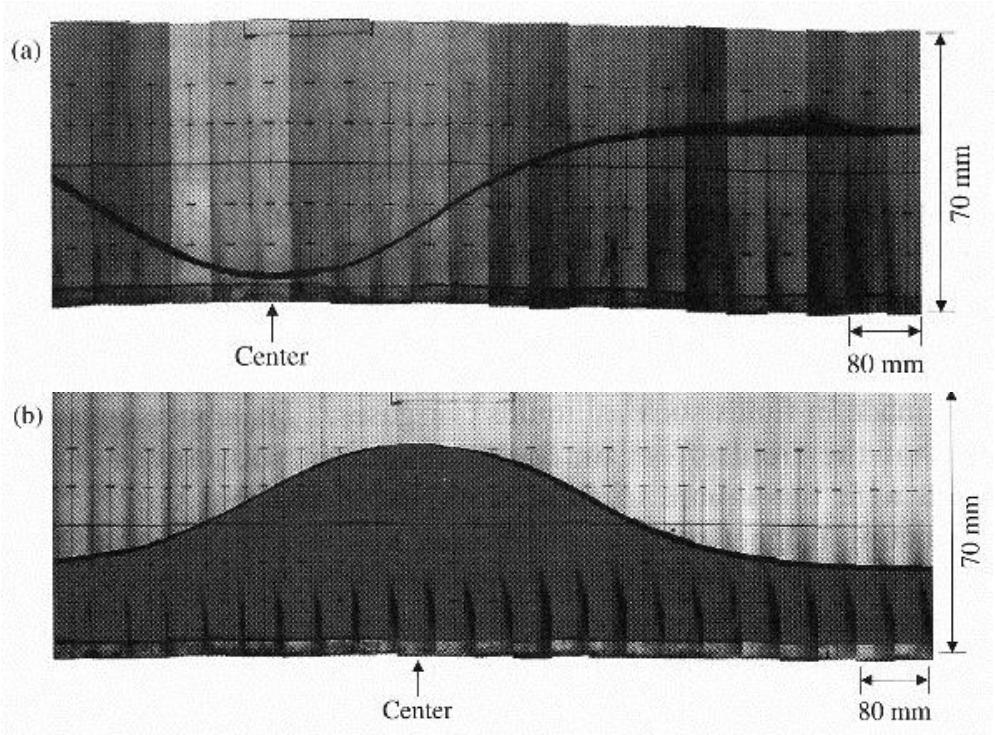

Figure 1.11 Moses effect and reversed Moses effect. Photographs of surface profiles of water (a) and copper sulfate aqueous solution (b) along bore (x) axis in a superconducting magnet. The applied field at the center was 10 T. The x direction is rescaled by 1/4. Difference of the liquid levels at the center and out of field was -38.9 mm for water, and 32.6 mm for copper sulfate aqueous solution.

Meanwhile, when a vessel containing water is placed in a horizontal high magnetic field gradient, water is split into two parts, because water is repelled out from magnetic field. [35] In contrast, the surface of a nearly saturated copper sulfate aqueous solution is raised at the magnetic field center. This phenomena are known as the “Moses effect” and the “reversed Moses effect” as shown in figure 1.11. [36] Furthermore, the diamagnetic levitation and the Moses effect can be enhanced by using a counter paramagnetic liquid. This is called the magnetic Archimedes effect analogous to the usual Archimedes effects. [37]

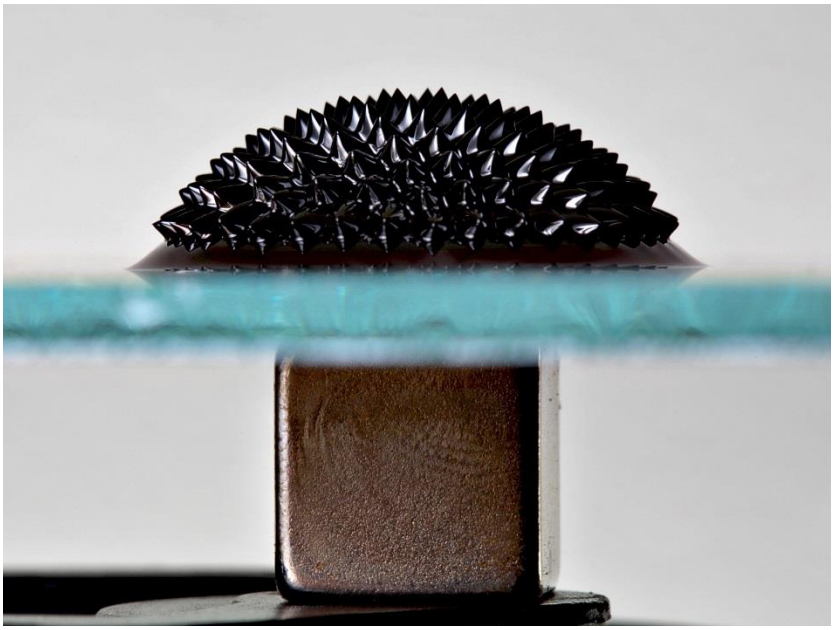

Figure 1.12 Photograph of a ferrofluid on glass plate and subjected to a magnetic field generated by the magnet underneath.

In addition, the fluid motion of ferrofluid can also be controlled by the induced magnetic force. [38] Ferrofluids are colloidal liquids made of nanoscale ferromagnetic particles suspended in a carrier fluid (usually an organic solvent or water). Each tiny particle is thoroughly coated with a surfactant to inhibit clumping. Ferrofluids usually [39] do not retain magnetization in the absence of an externally applied field and thus are often classified as "superparamagnets" rather than ferromagnets. The suspended miro-magnets in the ferrofluid respond to the external magnetic field by orienting along the field and, as a result, the field can exert strong forces on the fluid, radically changing its shape as the fluid moves to maximally fill its volume with magnetic field, as shown in figure 1.12.

1.4 Studies of fluid behavior under high magnetic fields

To improve the magnetic control of fluid flow, a number of efforts have been so far devoted to study the fluid behavior in magnetic fields. [40,41] Especially, with the remarkable progress recently in the superconducting magnet fabrication technology, the high magnetic field in large-scale room-temperature space can be obtained easily. The high magnetic field provides us more opportunities to study the fluid behavior in the magnetic field especially for feeble magnetic fluid. The recent research progress on fluid behavior in magnetic fields is briefly reviewed here.

1.4.1 Electric non-conducting fluids

For the flow control of non-conducting fluid, investigations so far mainly focused on the utilization of magnetic force. The Lorentz force acted on non-conducting materials is quite weak due to their low electrical conductivity. While the magnetic force can be acted on all kinds of materials depends on their magnetism and magnetic field gradient.

Under gradient magnetic fields, one can control buoyancy-driven convection in non-conducting fluids (for example pure water) by balancing buoyancy convection and magnetic convection. If the magnetic field gradient coexists with the magnetic susceptibility gradient in a fluid, the convection in the fluid can be controlled by the induced magnetic force. For the paramagnetic fluid whose magnetic susceptibility is followed Curie's law, the gradient of the magnetic susceptibility caused by the temperature gradient across the fluid can create a fluid motion dependent on the magnetic force. [42] For a diamagnetic fluid whose magnetic susceptibility is dependent on the density, the gradient of the magnetic susceptibility caused by the density difference can also modify the convection in terms of the magnetic force. [43] In the case of ferrofluid, a convective flow, called thermomagnetic convection, can be drove by induced magnetic force under an external uniform magnetic field when magnetization gradient was caused by spatially varied temperature distribution in the fluid. [38]

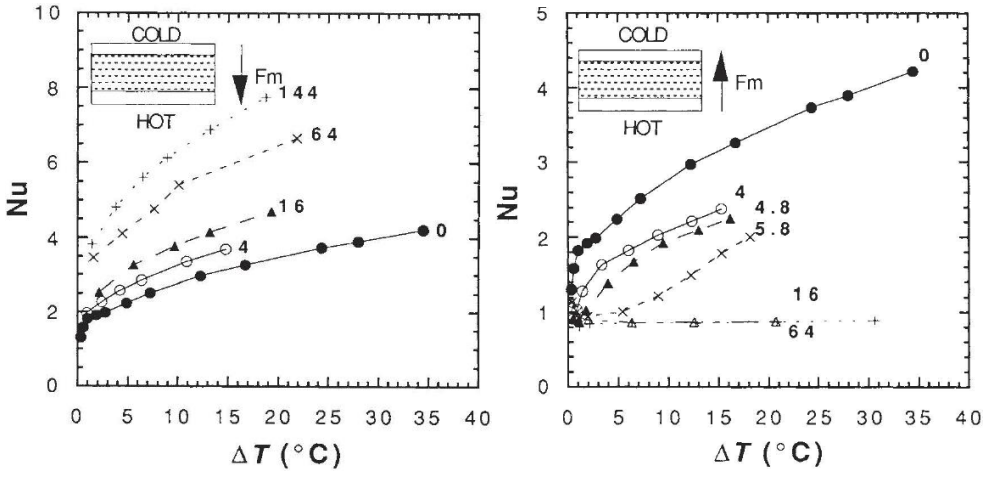

(a) (b)

Figure 1.13 Nusselt number as a function of temperature difference for gadolinium nitrate solution layer. Numbers represent the value of $\mu_0{}^2H(\mathrm{d}H/\mathrm{d}z)$, in units of T^2/m, for each curve, and the insets show the experimental configuration. The sample fluid layer was heated from below and cooled from above in both cases. The magnetic force was applied downwards in (a) and upwards in (b). In the latter case, the natural convection is inhibited by the field, and is suppressed totally for $\mu_0{}^2H(\mathrm{d}H/\mathrm{d}z) > 15\ \mathrm{T}^2/\mathrm{m}$.

The paramagnetic gases and liquids were initially studied. Braithwaite et al. [44] investigated convection in a solution of gadolinium nitrate (paramagnetic, the magnetic susceptibility at room temperature is $1.63 \times 10^{-7}\ \mathrm{m}^3/\mathrm{kg}$) in a system comprising a horizontal fluid layer heated from below and cooled from above (Rayleigh-Benard system) in a magnetic field. They produced both the enhancement and suppression of the buoyancy-driven convection due to the magnetic field gradient, as shown in figure 1.13. Uetake et al. [45] put a ceramic tube in a high magnetic field and heated one part of the tube to produce a thermal convection of air (paramagnetic, the volume magnetic susceptibility at room temperature is 0.38×10^{-6}). By adjusting the position of the heating center in the magnetic field to control the direction of magnetic force acting on the air, the thermal convection was either accelerated or suppressed. Theoretical studies [46, 47] were also developed to understand and predict the paramagnetic fluid behavior in magnetic field. Huang et al. studied the effect of a static, nonuniform magnetic field on a laterally unbounded non-conducting paramagnetic fluid layer heated from below or above using a linear stability analysis of the Navier-Stokes equations

supplemented by Maxwell's equations and the appropriate magnetic body force [48], and showed that the convective heat transfer of electrically non-conducted paramagnetic fluid can be effectively controlled by a non-uniform magnetic field [49]. Tagawa et al. [50] modeled the magnetic force by considering magnetic susceptibility as a function of temperature and included it in a momentum balance equation as an external force term in addition to the buoyant force term. It was found that the magnetic force acts on material of high magnetic susceptibility, like oxygen gas in a temperature gradient field, and affects the convection in addition to gravity. Fornalik et al. [51, 52] experimentally studied the flow of paramagnetic fluid ($Gd(NO_3)_3 \cdot 6H_2O$ solution) inside a cylinder placed in a bore of a superconducting magnet. Wrobel [53, 54] experimentally and numerically analyzed the influence of a strong magnetic field gradient on convection process of paramagnetic fluid in the annulus between horizontal concentric cylinders. Under strong magnetic fields, Poodt and coworkers have visualized the flow and solute concentration distribution around $NiSO_4 \cdot 6H_2O$ [55, 56] and lysozyme [57, 58] crystals based on Schlieren technique. As shown in Figure 1.14, a convection plume was observed under normal gravity condition, but not appeared under effective microgravity condition.

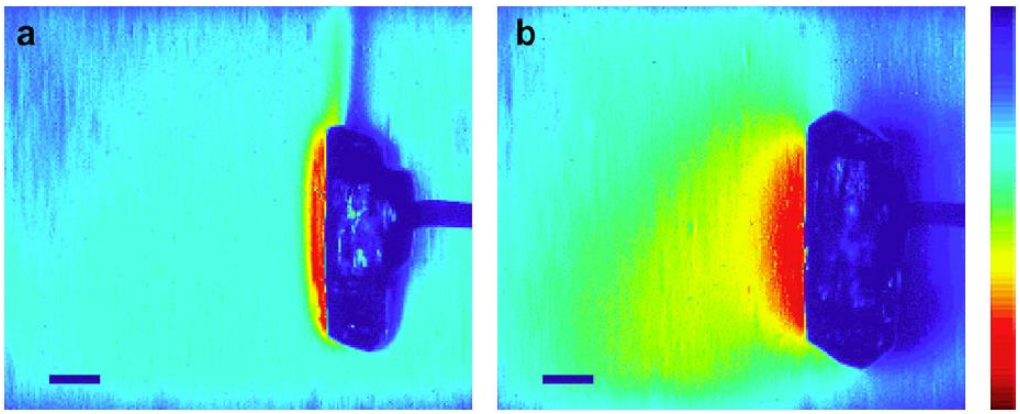

Figure 1.14. False color Schlieren image of growing $NiSO_4 \cdot 6H_2O$ crystal under normal gravity (a) and effective microgravity (b). The convection plume was observed in (a) but not in (b). The scale bar corresponds to 0.5 mm. [55]

In regard to convection in diamagnetic fluids, several theoretical studies [59-64] modeled the magnetic force by considering magnetic susceptibility as a function of density which is dependent on the temperature or concentration, and predicted that the convection can be either enhanced or suppressed by a magnetic force. Qi et al. [60] calculated the effects of the non-uniformity (3-4%) of a magnetic field strength in a radial direction of a solenoid type magnet on buoyancy convection. In figure 1.15, the temperature of the center of the container bottom was 2°C higher than other areas of the container. With increasing magnetic field intensity, the magnetic force imposed in a radial direction by the non-uniformity significantly changed the pattern of the convection inside container (1 cm in height and 2 cm in diameter). Wakayama [65, 66] studied the mechanism of the dampening effect of magnetic field gradients, $B(dB/dz)$, on solute convection and calculated the magnitude of $B(dB/dz)$ required for dampening. When the absolute value of mass magnetic susceptibility of a solute was about 70% of that of a solvent (e.g., KCl crystal growth from an aqueous solution) and the weight ratio was 0.26, the gradient to damp convection considerably was estimated to be -3018 T^2/m. On the other hand, when the mass magnetic susceptibility of the solute is nearly equal to that of the solvent [protein crystal growth (lysozyme)], a gradient of -1394 T^2/m damps convection completely on the

earth. Further numerical simulations [67-70] were also carried out to study the flow and concentration distribution in crystal growth processing under strong magnetic field.

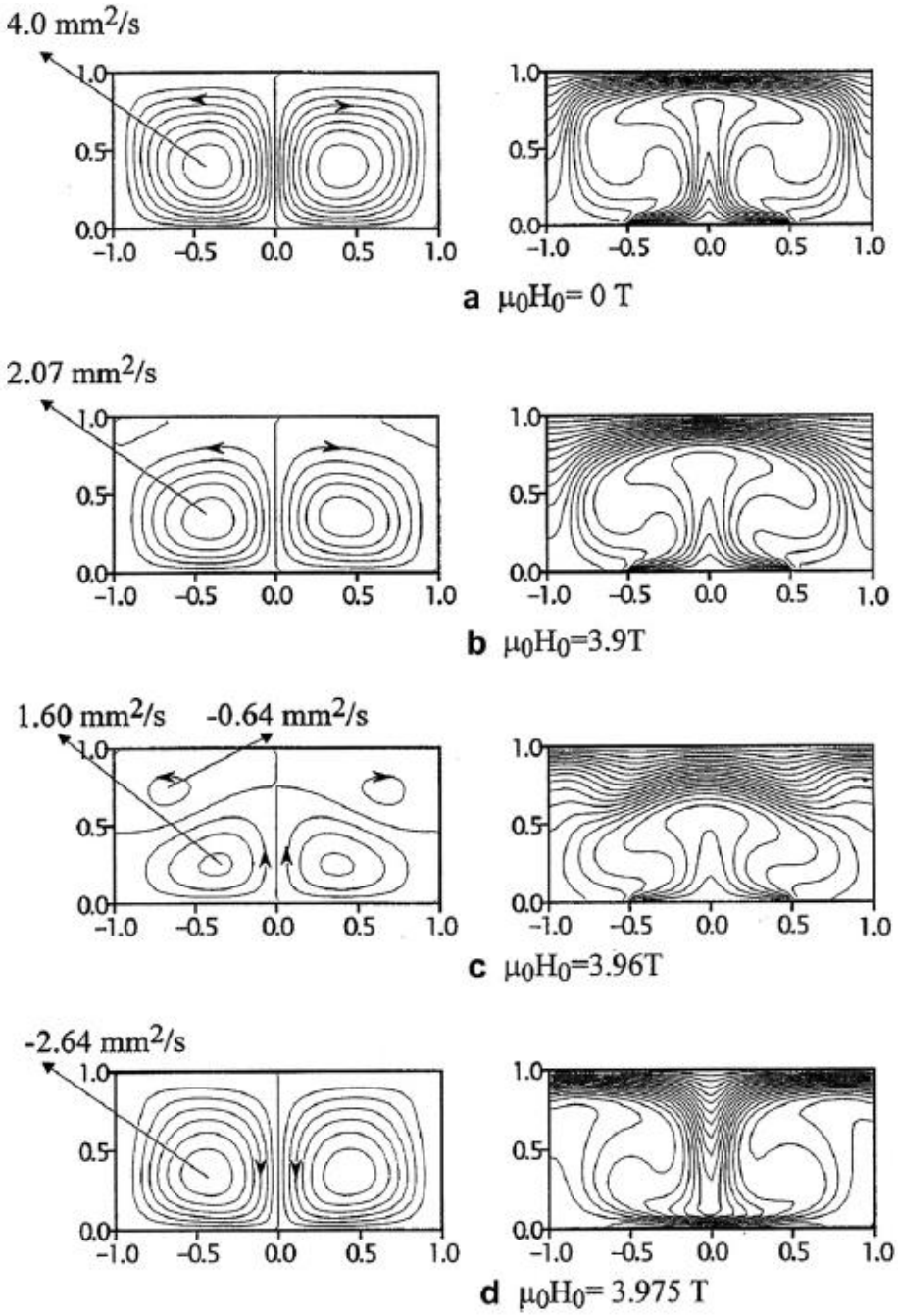

Figure 1.15 Effects of non-uniform magnetic fields, generated with a solenoid-type magnet, on buoyancy convection. Streamlines (left) and temperature contours (right) for different field strengths ($\mu_0 H_0$). The site coordinates of the vertical and horizontal axes are shown in centimeters units.

Recently, the magnetic force effect on convection in diamagnetic fluid has been confirmed by experimental studies. Nakamura et al. [71] configured a system of a horizontal fluid layer heated from below (also Rayleigh-Benard convection system) to investigate the effect of the magnetic field on convection in water (diamagnetic, the magnetic susceptibility at room temperature is -9.1×10^{-9}

m^3/kg). By measuring the temperature difference using thermocouples and observing images of convection patterns based on the shadowgraph technique, they found evidence that convection in diamagnetic fluids can be either suppressed or enhanced depending on magnetic force direction. Figure 1.16 shows the shadowgraph images of convection patterns near the onset of convection driven by the magnetic force.

To obtain a larger volume of effective microgravity by applying magnetic forces, superconducting magnets that provide uniform magnetic forces have been developed. [72-76] Although such superconducting magnets are few, crystallization experiments using such magnets are dramatically lower in cost than experiments using real microgravity environments in space and hence are expected to be developed in the future.

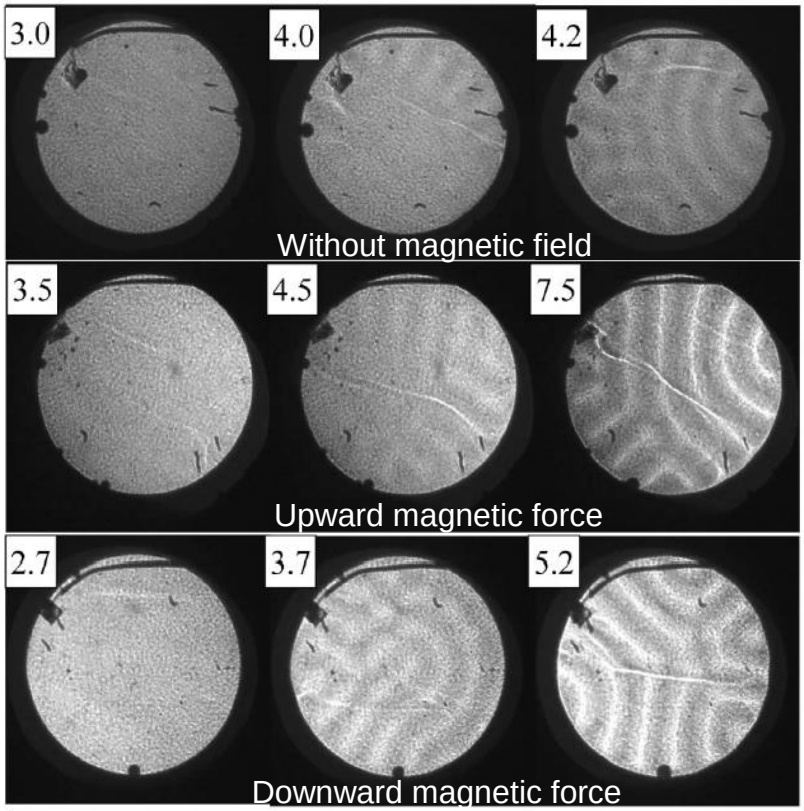

Figure 1.16 Shadowgraph images of convection patterns near the onset of convection. The number in each square is the value of ΔT (°C) across the fluid. Convective patterns appear at large ΔT under the upward magnetic force but at small ΔT under the downward magnetic force.

In the case of ferrofluid, the convective instability of ferromagnetic fluid layer heated from below in the presence of a uniform vertical magnetic field was first theoretically predicted by Finlayson. [77] Then, Schwab [78,79] presented the experimental evidence for such prediction by examining the influence of a homogeneous vertical magnetic field on the onset of Benard convection in a ferrofluid layer. The existence of pure thermomagnetic convection was also experimentally proven by Odenbach [80] under microgravity conditions. Luo et al. [81,82] also found that multiple instabilities of a horizontal ferrofluid layer can occur in the presence of oblique and vertical magnetic field. Furthermore, Engler et al. [83-85] developed a heat transfer measurement experimental setup and

discussed about the influence of a time-modulated driving force on the convection and the critical Rayleigh number in a ferromagnetic fluid. Based on this experimental setup, Heckert [86] studied the influence of ferromagnetic fluid composition on onset of thermomagnetic convection in vertically applied magnetic field. Namely the EMG905-fluid and the NF4000C-fluid, both kerosene-based magnetite fluids, were investigated at various magnetic field strengths and temperature differences. As an example, figure 1.17 shows the relationship of the heat flux density through a layer of EMG905-fluid of a thickness of 2 mm against the temperature difference for various values of the inner magnetic field strength in the layer. In the case of positive temperature gradient (heat from below, figure 1.17 a), all curves deviate at a critical temperature difference (onset of convection) which decreases with increasing magnetic field. For the case of fluid layer heated from above (negative temperature gradient), the transition from conduction to convection only takes place in the presence of magnetic fields as shown in figure 1.17 (b). For the NF4000C-fluid, similar behavior was observed.

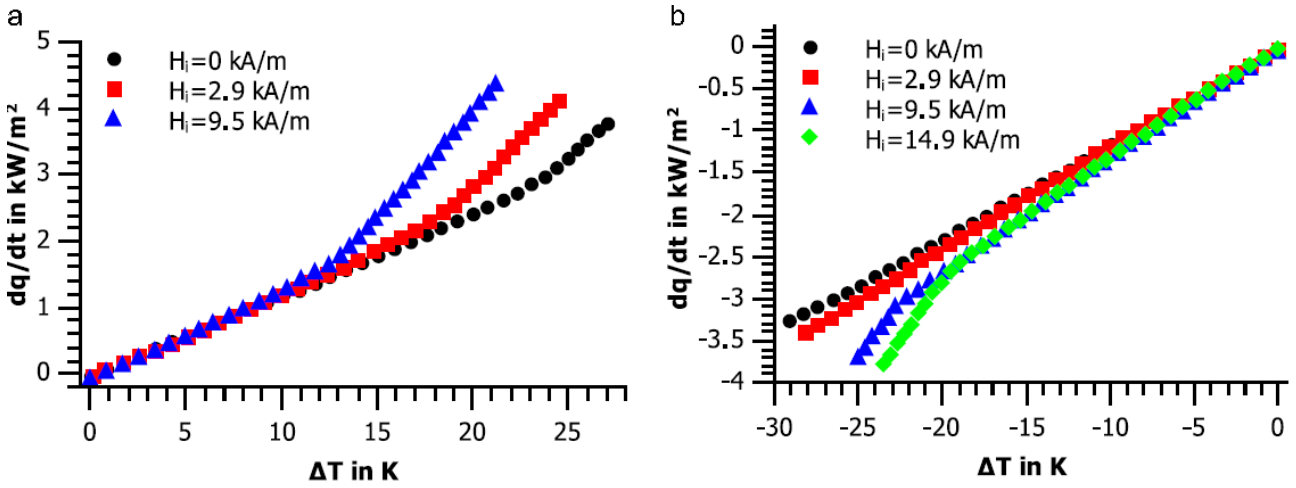

Figure 1.17 Heat flux density q through a 2 mm layer of EMG905-fluid when heated from below (a) and above (b) for various inner magnetic field strengths H_i. Deviation from reproductive measurements lies within the size of the symbols. [86]

Beside the theoretical investigations which done by Finlayson [77], further theoretical studies have been carried out by Huke et al. [87] and Laroze et al. [88]. These works mainly focused on different pattern formations while the convection was present. Relative experimental investigations have been carried out by Berkovsky et al. [89].

1.4.2 Electric conducting fluids

For the fluid with a high electric conductivity, such as liquid metal, the fluid motion can be effectively suppressed by applied Lorentz force in the presence of a magnetic field. [90,91] It is an established physical and there have been much experimental evidences support this conclusion.

Chandrasekhar theoretically analyzed the effects of magnetic field on the suppression of thermal convection in conductive fluids. [92] Then Nakagawa [93] and Jirlow [94] provided experimental evidence for the inhibition effect of magnetic field on convection in mercury layer. Based on this phenomenon, Utech and Flemings [95] successfully eliminated solute banding caused by turbulence

convection in a Te-doped InSb crystal by applying a magnetic field during crystal growth. The success of such attempt led to the novel insight that the use of a high uniform magnetic field can significantly suppress the fluid flow in a conducting melt in terms of Lorentz force. [96-102]

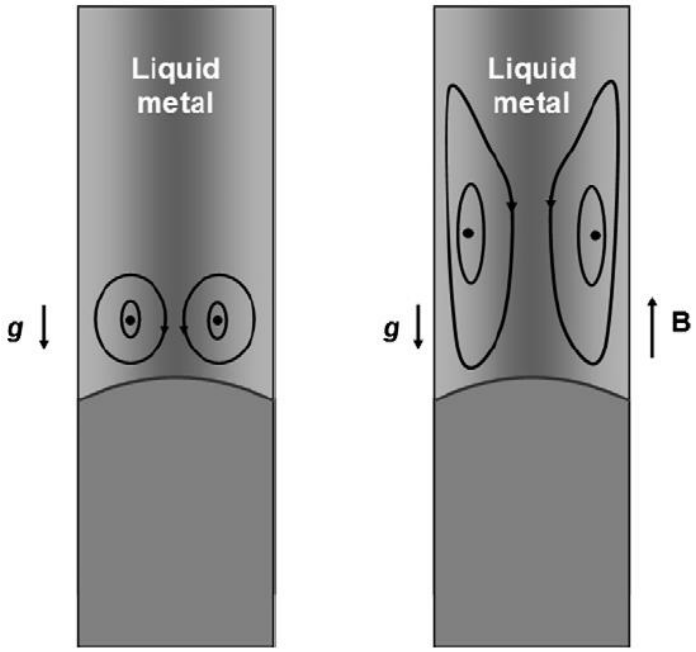

Figure 1.18 Stretching of the conductive loops in a vertical Bridgman furnace under a vertical magnetic field treatment. [107]

Following their work, extensive numerical and experimental investigations were conducted to examine the effects of magnetic field on the flow structure and stability of liquid metals. [103-125] Oreper and Szekely [103] reported that the natural convection can be suppressed by applied magnetic field and the extent to that the suppression effect depends on the strength of the magnetic field. Venkatachalappa et al. [104] presented numerical results for a fluid in a rectangular enclosure in a vertical magnetic field with uniform heat flux from the side wall. The results show that the temperature and velocity fields were significantly affected by the application of magnetic field. Rudraiah et al. [105] also confirmed this modification and further suggested that the rate of heat transfer was decreased through suppressing convection. Kakarantzas et al. [106] studied the natural convection of liquid metal in a vertical annulus with lateral and volumetric heating in the presence of a horizontal magnetic field by performing three-dimensional direct numerical simulations. Gaxandet et al. [107] reported that, in the Bridgman growth processing, the convective loops will be stretched along the magnetic field until it reaches the whole length of the liquid region, to minimize the velocity gradient, as shown in figure 1.18. In his report, it was also observed that the loop center moves to the wall and the return path of the liquid metal becomes smaller and the radial flow is constrained. Moreover, in both vertical and horizontal Bridgman processes, it has been proven that an imposed magnetic field leads to suppressing the macroscopic flow and thermal instabilities, resulting in a more homogeneous growth. [108] Some of the other numerical studies have also been made to examine the effects of magnetic field on Czochralski crystal growth and other phase change problems. The numerical results showed that the oscillatory flow in the Czochralski melt can be suppressed by applying a magnetic field. [109] Furthermore, the suppression is strongly dependent on magnetic field

direction, namely, an external magnetic field aligned perpendicular to the heated vertical wall was found to be more effective than a field applied parallel to the wall. [110] For the Czochralski growth of large diameter (> 300 mm) crystal, the application of a cusp magnetic field has also been paid much attention due to the three-dimensional control of the distribution of the magnetic flux density in the melt. [111-113]

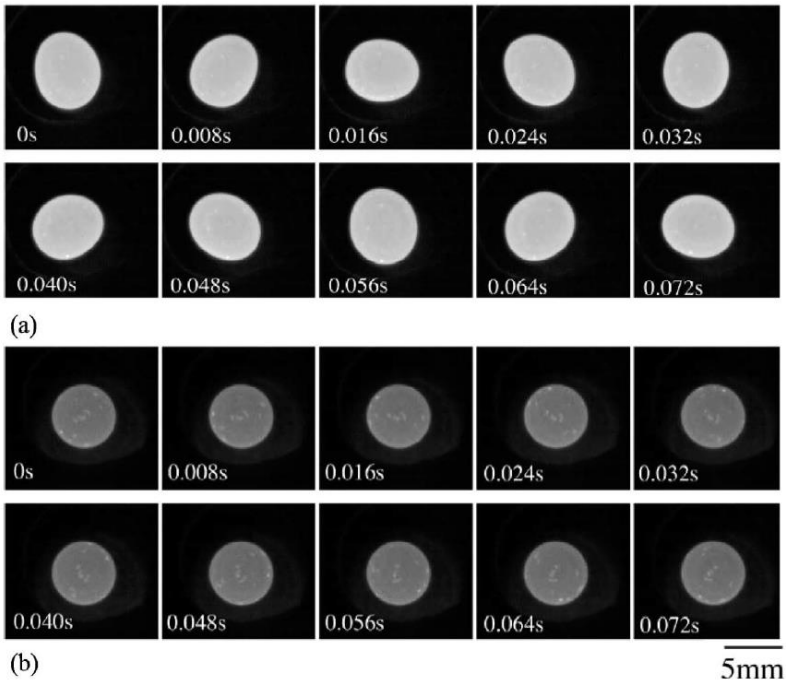

Figure 1.19 Sequence of levitated Cu melt shape in a static magnetic field of (a) 0 T and (b) 10 T. The interval between frames is 8×10^{-3} s. [124]

As described above, the studies based on numerical simulation were the main player in understanding the conductive fluid behavior in magnetic field, and there are a limited number of s experimentally obtained on the behaviors of conductive melts in magnetic fields. The main reasons for this is that, since most of studies related with conductive fluid flow control focused on the behavior control of liquid metal, and liquid metals appear at very high temperatures and have very low light transparencies, measuring and visualizing the behaviors liquid metal in magnetic fields are quite difficult. In order to further optimize the magnetic control of conductive fluid behaviors, the experimental evidence is extremely important but still lacked.

There are already some efforts have been devoted to experimentally observed the fluid behavior of liquid metal in the magnetic fields. Some previous experimental investigations [110,114-122] have focused on temperature measurements from which magnetic suppressing effects are deduced. For example, Okada and Ozoe measured temperature profiles in molten gallium contained in a cubic cavity and confirmed the suppression of natural convection induced by temperature gradients using a magnetic field. [110] Kaneda et al. [121] studied the natural convection of liquid gallium under uniform magnetic field with an imposed electric current by temperature measurement combined with numerical simulation. With the help of the hot-wire probe technique, Xu et al. [122] obtained direct measurements of the melt flow velocity in molten gallium with and without an imposed magnetic

field. Magnetic field suppression of convection was observed in both the measured velocity and temperature profiles. Bonvalot et al. [123] and Yasuda et al. [124] investigated experimentally high magnetic field suppression of convection in metallic melts using a magnetic levitation method. In the work of Yasuda et al. [124], they observed using a CCD camera the motion of Cu and Ni melts which were levitated by the simultaneous imposition of static and alternating magnetic fields. Figure 1.19 shows the shape sequence of the levitated Cu melt. By applying a static magnetic field, suppression can be seen in the oscillations, convection, and rotations about axes perpendicular to the static magnetic field direction. More recently, in the study of Yanagisawa et al. [125], they reported the behavior of Rayleigh-Benard convection in liquid gallium under the influence of a horizontal magnetic field. The flow pattern was visualized by the measurement of ultrasonic velocity profiler and showed a suppression of oscillatory motion of the two-dimensional roll-like structure with increases in the intensity of the applied magnetic fields, as shown in figure 1.20.

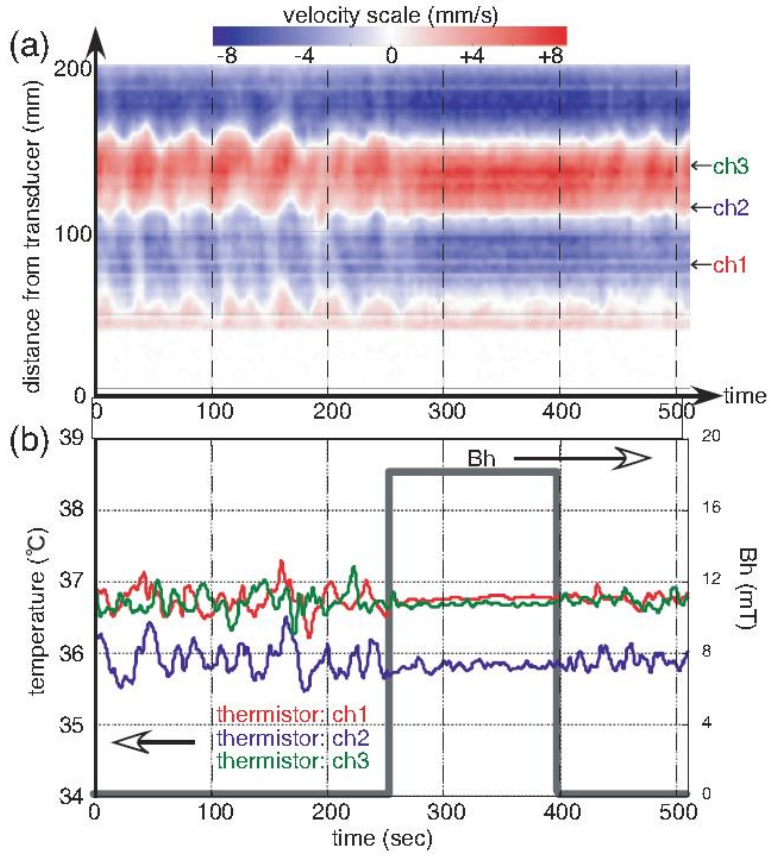

Figure 1.20 The behavior of the flow changes in response to abrupt increases and decreases in the horizontal magnetic field. Simultaneous measurements of (a) the horizontal flow velocities, and (b) the temperatures at the three positions, are shown with the intensity of the applied horizontal magnetic field *Bh* (b). The Ra for this case is 1.3×10^5. The direction and magnitude of the horizontal velocity are displayed in color scale.

However, although these works have presented some directly measurement of liquid metal flow in the magnetic field, the fluid behavior of molten metal still cannot be observed intuitively.

1.5 Motivation and objectives

The control of fluid flow is extraordinarily important for improvement of material quality. The application of magnetic fields has been regarded as an attractive means to control the convection of fluid. Since the magnetic control of fluid flow still has some limitations in practical processing. Considerable efforts have been so far devoted to study the fluid behavior in magnetic fields. Owing to these investigations the understanding of fluid behavior in magnetic fields has been deepen. Nevertheless, for the momentous magnetic control processing in melting metal, most studies are based on the numerical simulation, while the experimental evidence is quite limited. The fluid behavior of molten metal in magnetic field still cannot be well observed since the liquid metals appear at very high temperatures and have low light transparencies. However, such experimental evidence of magnetic field effect on fluid behavior in liquid metal is significant for the improvement of magnetic control processing.

Therefore, to solve the problem, the objective of my thesis is to improve the magnetic control of fluid flow by experimental observation of fluid behavior under high magnetic fields. In this thesis, not only the conductive fluid flow but also the non-conductive fluid flow were observed.

For the non-conductive fluid, the effect of the magnetic force is mainly considered. An *in-situ* optical observation system utilizable even under high magnetic field up to 13 T was developed based on Schlieren technique. The fluid motion of transparent solution can be visualized, without using the tracer, through the spatial distribution of the refractive index that depends on the concentration of solution.

For the conductive fluid, such as melt metal, the effects of Lorentz force and magnetic force are both considered. Since liquid metals normally appear in high temperature, the experimental observation is difficult. In this thesis, the electrolytes aqueous solution combined with a superconducting magnet is used as substitution, since flow conditions thereby are regarded as similar to those for liquid metals in industrial electromagnets. [127] Effects of magnetic fields on the thermal convection in conductive aqueous solutions at ambient temperatures are studied through heat transport measurements combined with shadowgraph technique-based visualization.

Chapter 2

Research methods

- **Superconducting magnet**
- **Schlieren technique**
- **Heat transport measurement with Shadowgraph-based visualization**

In this chapter, the experimental equipment including superconducting magnet and observation devices is described. The *in-situ* optical observation devices were developed based on Schlieren technique and shadowgraph technique, respectively. The principle of these techniques and the related experimental procedure are briefly introduced.

2.1 Superconducting magnet

In this thesis, two cryo-cooler operated type superconducting magnets were used for observation of fluid behavior under high magnetic fields. One can generate the magnetic field up to 13.0 T (JASTEC, model JMTD-10C13E-NC) and was used for experiments related with observation of non-conductive fluid. Another was used to generate magnetic fields up to 12.0 T (Sumitomo Heavy Industries Ltd., Model HF12-100VHT) for experiments related with observation of conductive fluid.

Both of the superconducting magnets were used in vertical direction to generate vertical magnetic field in the center. And all of them have a room temperature bore of 100 mm in diameter. In the bore of the magnets, the magnetic field varies spatially. Images of two superconducting magnets are showed in figure 2.1.

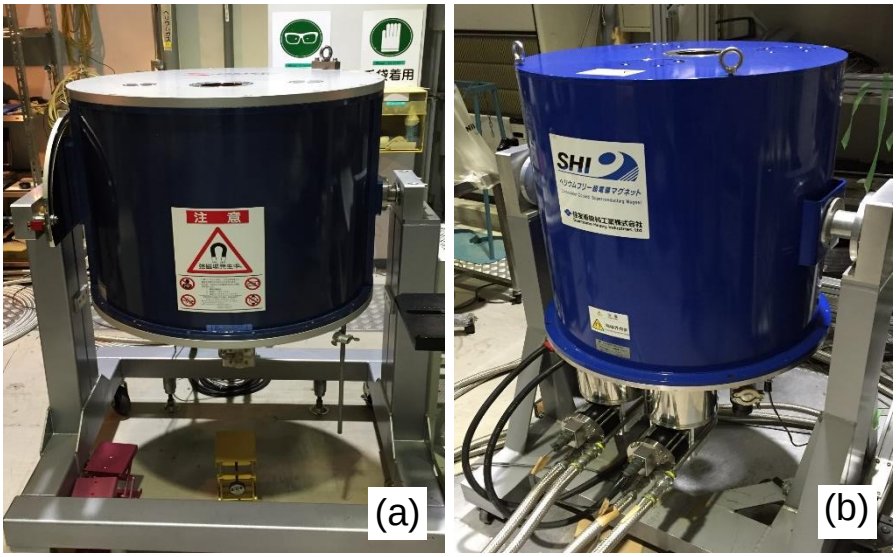

Figure 2.1 Images of superconducting magnets used in experiments: (a) 13.0 T, (b) 12.0 T.

2.2 Schlieren technique

2.2.1 Principle of Schlieren technique

Schlieren method is a technique that detects optical inhomogeneities in transparent refractive media and defects of reflecting surfaces. The principle of Schlieren technique is illustrated in figure 2.2. When the light go through an inhomogeneous media, it becomes bent because of the different refractive index in the media. As shown in figure 2.2 (a) the light comes from the light source go through a series of lenses and detection zone with a refractive index gradient, then focused by another

lens and received by the camera. A knife-edge is fixed at the focal spot. The upward-deflected ray brightens a point on the screen, but the downward-deflected ray hits the knife-edge. Its corresponding image point is dark against a bright background. For this particular point of the schlieren object, the phase difference causing a vertical gradient $\partial n/\partial y$ (n is the refractive index of media) in the test area is converted to an amplitude difference, and the invisible is made visible. Therefore, the distribution of refractive index in detection zone was displayed as a focused image, shown like figure 2.2 (b).

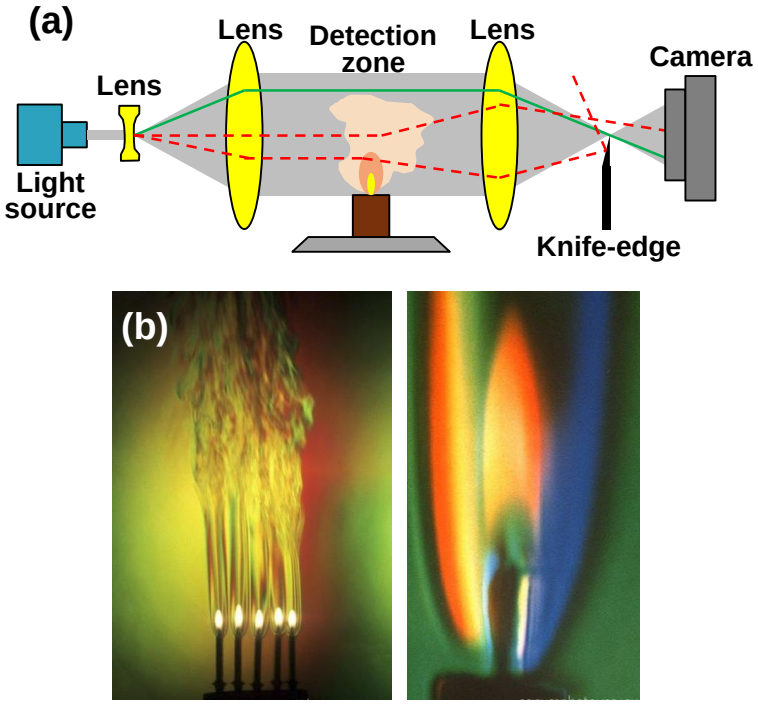

Figure 2.2 Schematic diagram of Schlieren method (a) and obtained Schlieren images (b).

Since the refractive index in transparent solution depends on the density gradient. The fluid motion with different density can be readily observed by using this Schlieren technique.

2.2.2 Equipment

Based on the Schlieren technique, *in-situ* optical observation device was developed and illustrated in figure 2.3 with superconducting magnet.

The halogen light (HIBIKI, H-150) was used as a light source. The light was introduced to the optics by using optical fiber. A series of lenses and mirrors were used to lengthen the light path and to make a Schlieren image. To record the Schlieren image, a CCD device (ELMO, UN43H) was used and a knife-edge was placed at a focal point just before the CCD. The light pass through the sample fluid in the holder fixed at a certain point in the magnet bore in horizontal direction.

To observe the behavior of non-conductive fluid utilizing this Schlieren device, the suspended crystal dissolution process was conducted. The sample crystal was first grown at the tip of a thin wire by recrystallization from the supersaturated solution. Then the obtained sample was introduced into a cubic glass container (sample holder, the size of this holder is 11.5×8.25×12.5 mm^3) and was

suspended around the center of the holder by using the thin wire. As surrounding solutions, water or low concentration solutions were used. Since the solute-rich solution appeared around the sample crystal when it began to dissolve, the buoyancy driven convection occurred due to the density difference between the solute-rich solution and the surrounding solution. Owing to the refractive index in transparent solution depends on the density gradient, the fluid motion during the dissolution process was therefore obtained by such *in-situ* optical observation system.

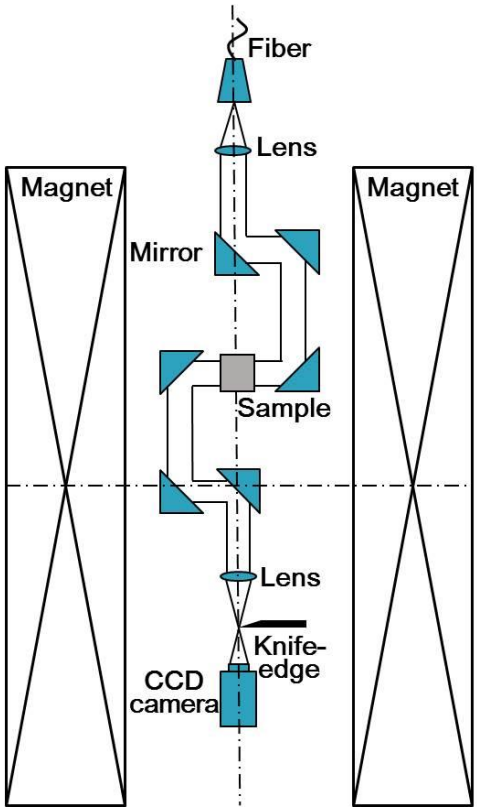

Figure 2.3 Schematic illustration of experimental configuration built based on Schlieren technique.

2.3 Shadowgraph technique

2.3.1 Principle of Shadowgraph technique

The shadowgraph technique is an optical method that reveals non-uniformities in transparent media like glass, water and air. The principle of shadowgraph technique was illustrated in figure 2.4. The parallel light passed through the detection zone projected on the screen directly. The irradiance depends on the second derivative of the refractive index in the detection zone. The differences in light intensity are proportional to the second spatial derivative (Laplacian) of the refractive index field in the transparent medium. Based on the shadowgraph technique, the fluid flow in a transparent media can also be observed by the flow pattern in the shadowgraph image as showed in figure 2.4 (b).

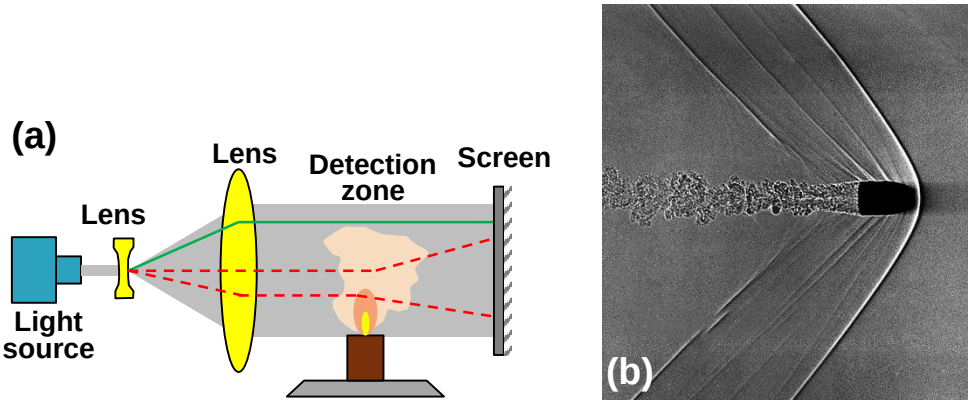

Figure 2.4 Schematic diagram of shadowgraph technique (a) and shadowgraph images (b).

Both Schlieren and shadowgraph methods are integrating optical systems that project line-of-sight information onto a viewing screen or camera focal plane. Although they are closely related, several distinctions are exist and have shown in table 2.1 [128]

Table 2.1 Distinctions between shadowgraph technique and Schlieren method.

Shadowgraph	Schlieren
Displays a mere shadow	Displays a focused image
Shows light ray displacement	Shows ray refraction angle
Illuminance level responds to the second spatial derivative or Laplacian, e.g. $\partial^2 n/\partial x^2$.*	Illuminance level responds to first spatial derivative of the refractive index, e.g. $\partial n/\partial x$.*
No knife edge used	Knife edge used for cutoff

* n is the refractive index of media.

2.3.2 Equipment

To study the fluid behavior in conductive solution under high magnetic fields, a system consisting of a superconducting magnet, an optical tower and a convection cell was built, as showed in figure 2.5.

In the experimental setup, a cryo-cooler operated superconducting magnet was used to generate magnetic fields up to 12.0 T. The convection cell contains a horizontal fluid layer heated from the bottom and cooled from the top (Rayleigh-Benard convection).

Sample fluids were first degassed by bubbling with argon gas, and then placed in a cylindrical convection cell with 40 mm in diameter and 4 mm in height. The side wall of the cell was made of Teflon with thickness of 4 mm. The top plate was made of sapphire with a thickness of 3 mm. For the bottom plate, aluminum or sapphire with an evaporated layer of gold on the surface to serve as a mirror were used for the heat transport measurement and the visualization experiment, respectively.

The top sapphire plate was cooled with circulating water, and the bottom plate was heated from below with a nichrome heater. The temperature of the circulating water was kept constant at 25.0°C. The temperature difference between the top and the bottom plates, ΔT, was measured by chromel-alumel thermocouples, one attached above the top plate and the other inside the bottom aluminum plate in the heat transport measurement, or below the bottom sapphire plate in the visualization experiment.

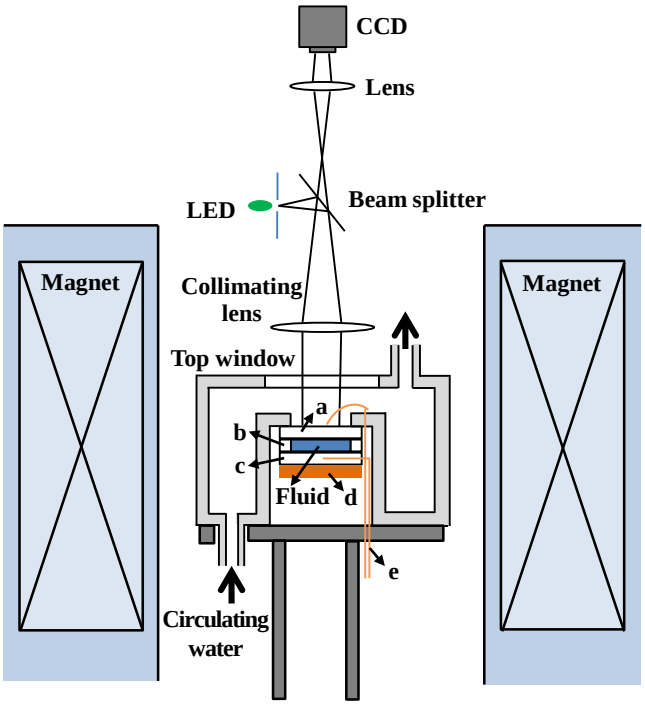

Figure 2.5 Schematic illustration of experimental setup built based on shadowgraph technique: (a) sapphire top plate, (b) Teflon ring, (c) aluminum or sapphire bottom plate, (d) heater, and (e) thermocouples.

The optical tower was mounted on the top of the convection cell for visualizing the flow by means of shadowgraph technique. The light from a bright LED was introduced into the convection cell, reflected by the bottom plate mirror, and finally projected onto a CCD camera. The whole observation apparatus was made of feeble magnetic substances for use in high magnetic fields, and installed in the magnet bore.

Based on this system, the heat transport measurement and flow visualization based on shadowgraph technique were conducted.

2.3.3 Rayleigh-Benard convection

In this experiment, the Rayleigh-Benard convection in the conductive fluid was induced and studied under high magnetic fields. [129,130]

When a horizontal fluid layer was heated from below and cooled from above, the induced thermal convection was called Rayleigh-Benard convection. The status of the fluid layer can be characterized by the dimensionless Rayleigh number, *Ra*, which is given by

$$Ra = \frac{g\beta\Delta T d^3}{\alpha v} \tag{2.1}$$

where g is the gravity acceleration, β is the coefficient of thermal expansion, d is the thickness of fluid layer, ΔT is the temperature difference across the fluid layer, α is the thermal diffusivity, and v is the kinematic viscosity. With heating the fluid layer from below and keeping the temperature from above, at first the heat transfer was dominated by heat conduction. Once the value of Ra exceeded a critical value Ra_c, corresponding to critical temperature difference ΔT_c, the thermal convection occurred. The heat transfer across the fluid layer was therefore changed from conduction to thermal convection.

2.3.4 Optical observation and heat transfer measurement

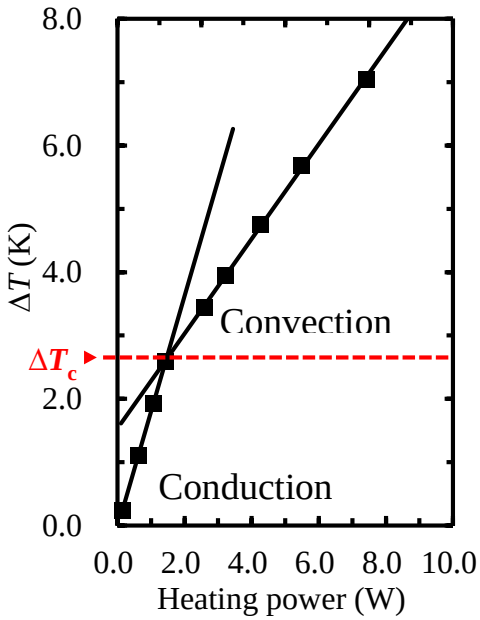

Figure 2.6 Temperature difference across the fluid layer, ΔT, versus the electric power generated by the bottom heater. The sample fluid was pure water here as an example. Solid lines were fitted with the least squares method

To evaluate the thermal convection in sample fluid, following procedure was adopted in the heat transport measurement. After the steady state was reached in the sample fluid layer, ΔT was first recorded without heating. Then, a certain amount of electrical power was supplied to the bottom heater, and ΔT was measured again after the steady state was reached. This procedure was repeated to obtain the relationship between ΔT and the supplied heater power, as plotted in figure 2.6 (using a sample fluid of water as an example).

It was clear seen form figure 2.6 that, the ΔT started to increase rapidly with increasing heater power at first. Then, this increase became moderate beyond a certain value of ΔT. The rapid increasing part corresponds to the region where the heat transport dominated by the heat conduction across the fluid. Once ΔT exceeded a certain critical value, convection occurred and became the dominant heat

transport process. Therefore, the slope of the ΔT – electric power curves become less steep; the solid lines are the best fits by the least square method. The critical temperature difference, ΔT_c, at the onset of convection, was determined by the intersections of these fitting lines. In this way the thermal convection in sample fluid was quantitatively evaluated.

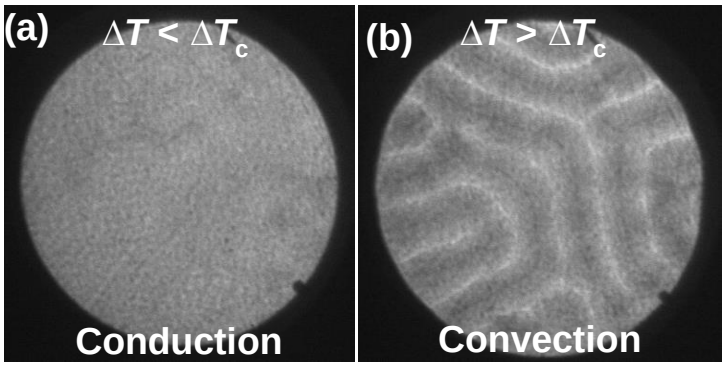

Figure 2.7 Shadowgraph images obtained before (a) and after (b) the convection occurred.

In case of the visualization experiment, shadowgraph images were recorded in each time when the steady state was reached in this procedure. Owing to the distribution of refractive index caused by thermal convection, the fluid flow can be visualized by flow patterns in the shadowgraph images as showed in figure 2.7.

Chapter 3

Effects on flow of non-conducting fluid

- **Schlieren technique-based visualization**
- **Magnetic force effect on flow direction**

In this chapter, the effect of high magnetic field on behavior of non-conductive fluid flow was investigated. Since the Lorentz force acted on material by magnetic field strongly depends on the electric conductivity of substance, the effect of magnetic force was the main player for the magnetic effects on non-conducting fluid. Numbers of efforts have been undertaken to understand the fluid behavior when the magnetic force was applied. [40-76] Owing to these efforts, understandings about the magnetic control of feeble magnetic fluid behavior have been deepened. However, there are still some phenomena not enough understood remaining, such as the fluid behavior in the solid-liquid coexisting system or the high temperature processing. Since the *in-situ* observation of phenomena under high magnetic fields gives us a lot of information, through the experimental observation in this chapter, we aim to contribute for development of the technique to control feeble magnetic fluid behavior using magnetic fields.

3.1 Experimental

For the experiment in this chapter, the *in-situ* optical observation system developed based on Schlieren technique were used combine with a 13 T superconducting magnet.

In the experiment, the dissolution process of an inorganic crystal suspended in a solution was observed. The material used here was Aluminium Potassium Sulfate 12-Water, $KAl(SO_4)_2 \cdot 12H_2O$. It is diamagnetic and its volume magnetic susceptibility is -1.149×10^{-5}. The solubility of this material in water is 140 kg/1 m^3-water at 20°C.

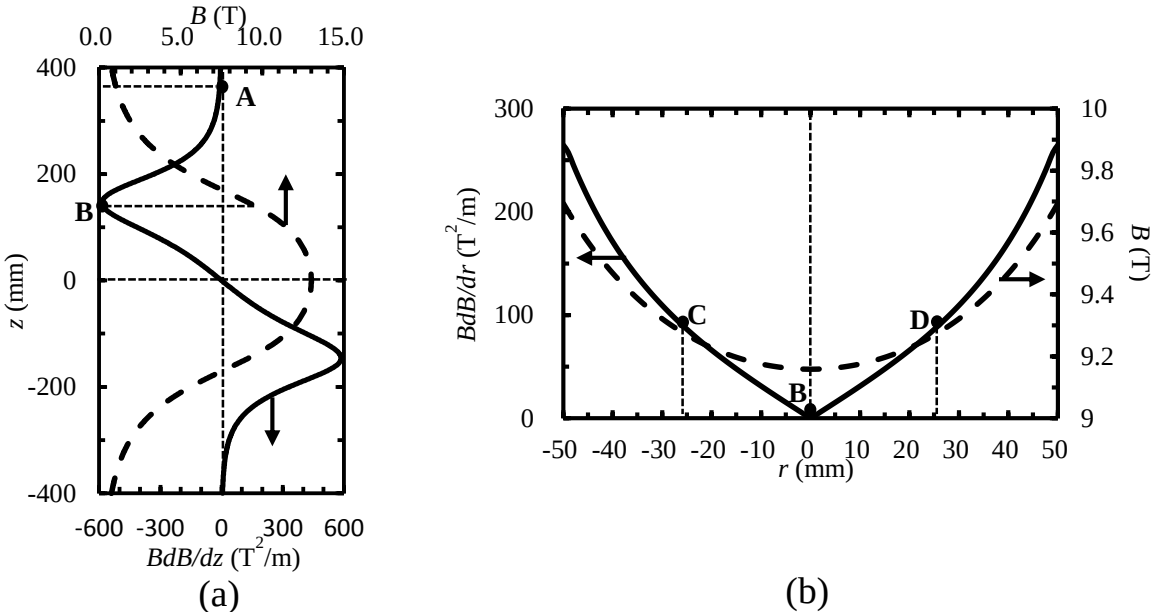

Figure 3.1 Spatial distribution of the magnetic field in the bore of the superconducting magnet (a) distribution of the magnetic field *B*, and the product of the magnetic field and the gradient of magnetic field, *B(dB/dz)*, along bore axis, (b) distribution of *B* and *B(dB/dr)* at z = 146 mm.

As surrounding solutions, distilled water (density $\rho = 0.998\times10^3$ kg/m^3, $\chi_w = -9.035\times10^{-6}$), quarter-saturated solution (3.72 wt%, $\rho = 1.010\times10^3$ kg/m^3, $\chi_{qs} = -9.07\times10^{-6}$) and half-saturated solution (7.03

wt%, ρ= 1.028×10^3 kg/m^3, χ_{hs} = -9.15×10^{-6}) of Aluminium Potassium Sulfate 12-Water were used. Densities of these solutions were measured and magnetic susceptibilities were calculated using the measured density and magnetic susceptibilities of water and Aluminium Potassium Sulfate 12-Water written in the literature.

Figure 3.1 shows the distribution of the magnetic field, *B*, and the product of the magnetic field and the gradient of magnetic field, *B(dB/dz)*, along bore axis (figure 3.1 a), and *B(dB/dr)* at *z* = 146 mm (figure 3.1 b). The maximum of *B(dB/dz)* is ±586 T^2/m at *z* = 146 mm. In figure 3.1 (b), *B* and *B(dB/dr)* were plotted for the range of -50 ≤ r ≤ 50. Intrinsically, in this coordinate system, -50 ≤ r ≤ 0 and 0 ≤ r ≤ 50 are equivalent. However, the point of observation is fixed against the bore space in this experiment, therefore, to distinguish the difference of experimental positions, *B* and *B(dB/dr)* were also plotted for -50 ≤ r ≤ 50.The sample holder was fixed at four different positions to see the effect of the spatial distribution of the magentic field.These positions are indicated in figure 3.1 by using symbols from A to D. Positions B to D were located at 146 mm above the magnetic field center (*z* = 146 mm), the maximum position of *B(dB/dz)*. Difference of these three points is the difference in horizontal location. Position B is located at the center (*r* = 0 mm), while positions C and D are located off-centered position, *r* = - 26 mm and 26 mm, respectively. *B(dB/dr)* values in these positions are 0 T^2/m for position B and 90.5 T^2/m for position C and D. The position A was selected as the control at *z* = 382 mm, where *B* = 0.88 T and *B(dB/dz)* = -6.6 T^2/m. The diamagnetic material receives an upward magnetic force at position B, C and D. The intensity of magnetic force, at position B, acting on water became around 40% of that of gravity force. In the radial direction, the direction of magnetic force acting on diamagnetic material always point to the center. In the position A, the magnetic force acting on diamagnetic material is negligibly small compared with the case in positions B, C, and D.

To eliminate the influence of the sample shape difference, a series of experiments was carried out in several positions sequentially with one sample. For example, in one case, the observation started at the point A, after waited for the stable condition, then, the sample was moved to the position B and waited for the stable condition, and repeated this sequence in a manner A, B, A, B …… continuously (pattern 1). In another case, a series of observation was carried out as a following sequence: A, D, A, C, A…… (pattern 2). Observed images in each position were compared to see the effect of the spatial magnetic field distribution on the flow of solution.

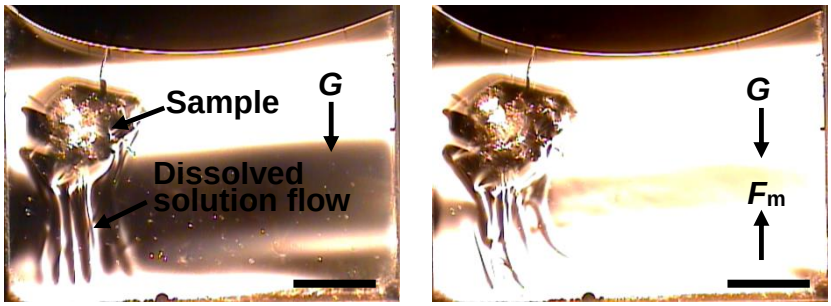

(a) (b)

Figure 3.2 Schlieren images obtained in the dissolution process of Aluminium Potassium Sulfate 12-water. Surrounding fluid is *water*.
(a) gravity condition (position A), (b) with magnetic field (position B, *B* = 8.97 T, *B(dB/dz)* = -586 T^2/m). The scale bar written in the images corresponds to 2 mm.

3.2 Results and discussion

Figure 3.2 shows the Schlieren images observed in the pattern 1 experiment. Figure 3.2 (a) and (b) were obtained at the position A and B, respectively. In this experiment, water was used as the surrounding fluid. The sample crystal of Aluminium Potassium Sulfate 12-Water was suspended left side in the sample holder. The concentration gradient is clearly visible as the lighter and darker patterns in images. The sample was slowly dissolved and the high concentration solution flow occurred toward downward. Without magnetic field, this dissolved solution flow fell down straightly toward the bottom of the sample holder as seen in Figure 3.2 (a). On the other hand, in the magnetic field, this dissolved solution flow was slightly bended as seen in figure 3.2 (b). In the subsequent process of this experiment, this phenomenon always appeared under magnetic field condition and disappeared under gravity condition. Using the quarter-saturated solution as the surrounding fluid, this bent of downward solution flow became smaller as shown in figure 3.3, and in case of the half-saturated solution, it almost disappeared as shown in figure 3.4.

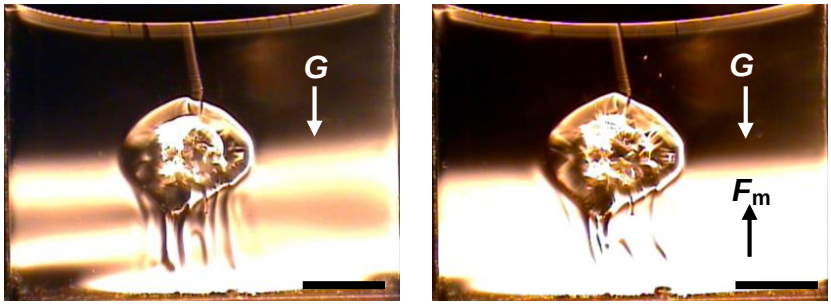

(a) (b)

Figure 3.3 Schlieren images obtained in the dissolution process of Aluminium Potassium Sulfate 12-water. Surrounding fluid is the *quarter-saturated solution*.
(a) gravity condition (position A), (b) with magnetic field (position B, B = 8.97 T, $B(dB/dz)$ = -586 T^2/m). The scale bar written in the images corresponds to 2 mm.

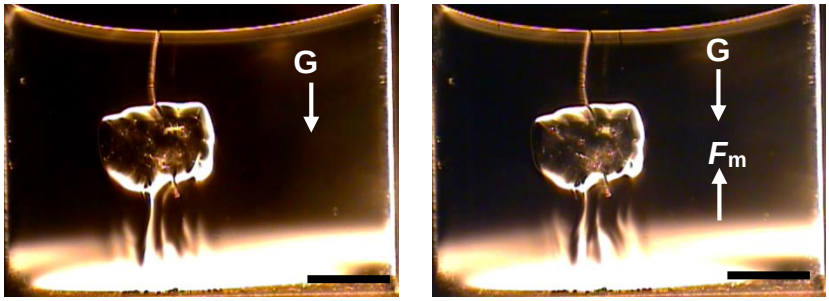

(a) (b)

Figure 3.4 Schlieren images obtained in the dissolution process of Aluminium Potassium Sulfate 12-water. Surrounding fluid is the *half-saturated solution*.
(a) gravity condition (position A), (b) with magnetic field (position B, B = 8.97 T, $B(dB/dz)$ = -586 T^2/m). The scale bar written in the images corresponds to 2 mm.

Figure 3.3 shows a series of Schlieren images obtained in the pattern 2 experiment. Numbers written under the images represent the elapsed time from the beginning. The surrounding medium was water also in this experiment. The experiment was started at the position A, gravity condition. As observed in the previous case, the downstream of dissolved solution flow was straight. When the sample was moved to the position D, this downstream was bended toward left side, the direction of the bore axis (r = 0 mm). After moved back to the position A, it returned to the original straight stream. Then, after moved to the position C, the direction of downstream was bended toward right. This is also the direction of the bore axis. In this experiment also, degree of bent became smaller in the quarter-saturated solution and almost disappeared in half-saturated solution. Each series of experiment in this chapter was repeated several times and similar results were obtained.

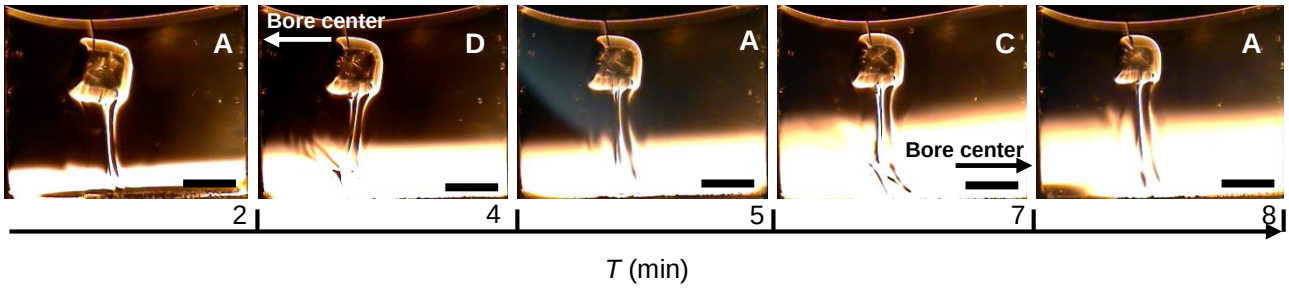

Figure 3.5 Schlieren images obtained in the dissolution process of Aluminium Potassium Sulfate 12-water under different magnetic field conditions. Surrounding fluid is water.
(a), (c), (e): gravity condition (position A), (b): condition that vertical and horizontal (in the direction from right to left) magnetic force acting on diamagnetic fluid (position D); (d) condition that vertical and horizontal (left to right) magnetic force acting on diamagnetic fluid (position C, $B(dB/dr)$ = 90.5 T^2/m). The scale bar corresponds to 2 mm.

In this experiment, the behavior of the downward flow of high concentration solution in the sample dissolution process were observed with Schlieren device when the sample was suspended in water, quarter-saturated solution and half-saturated solution. All materials involved in this experimental system were diamagnetic materials. Under spatially varied magnetic field, all these materials experienced the magnetic force toward the direction that the magnetic field decreasing. Therefore, the effect of the magnetic force became relative one. With changing the concentration of the surrounding fluid from water to half-saturated solution, the difference of magnetic susceptibilities between high concentration solution and surrounding fluid getting small. The degree of the observed bent of the downward flow direction decreased with decreasing the magnetic susceptibility difference, therefore, the mechanism of this phenomenon seems to be related to the magnetic force. Indeed it was confirmed that the direction of the bent of the downward flow became opposite when the spatial distribution of the magnetic field in horizontal direction was reversed, as seen in figure 3.3 (b) and (d).

In here, let us consider about the force acting on the high concentration solution that flows downward in the sample dissolution process. We assumed that this high concentration solution was the saturated solution of Aluminium Potassium Sulfate 12-Water. The density and the magnetic susceptibility of the saturated solution are 1.056×10^3 kg/m^3 (measured), and -9.253×10^{-6} (calculated),

respectively. Then, the force acting on unit volume of the saturated solution surrounded by the other fluid in vertical direction is expressed as follows:

$$F_v = -(\rho_s - \rho_w)g + \frac{(\chi_s - \chi_w)}{\mu_0} B \frac{dB}{dz} \tag{3.1}$$

where ρ_s is the density of the saturated solution, ρ_w is the density of the surrounding solution, χ_s and χ_w are magnetic susceptibilities of the saturated and the surrounding solutions, respectively, and g is the gravitational acceleration. In this experimental system, the saturated solution is more diamagnetic compared with the surrounding solution, therefore, the magnetic force acting on the saturated solution direct upward and is worked as magnetically induced buoyant force (magento-Archimedes buoyant force). [37] The intensity of this magnetically induced buoyant force becomes about 18% of that of the gravitational force. This seems relatively large force. The velocity of the downward flow might be affected by the magnetic force, however, it is very difficult to distinguish by Schlieren technique because this method is not suitable for quantitative evaluation.

On the other hand, the force acting on unit volume of the saturated solution surrounded by the other fluid in horizontal direction is expressed as follows:

$$F_r = \frac{(\chi_s - \chi_w)}{\mu_0} B \frac{dB}{dr} \tag{3.2}$$

Considering the spatial distribution of the magnetic field in horizontal direction (figure 3.1(b)), the magnetic force was exerted to the saturated solution that is more diamagnetic against the surrounding fluid, toward the direction of the bore axis. It means that the direction of the magnetic force was leftward in case of the experiment in figure 3.3 (b) and was rightward in case of figure 3.3 (d). This consideration is fit with the experimental observations. When water was used as the surrounding fluid, the intensity of this horizontal magnetic force becomes about 3.3% of the gravity force in vertical direction. This is not large compared with the magnetic force acting on the saturated solution in vertical direction. However, in the horizontal direction, only the magnetic force was acting on the saturated solution, therefore, the bend of the downward flow could be observed sensitively.

Incidentally, the bend of the high concentration downward flow was observed also in the experiment at the position B as seen in figure 3.2 (b). In this experiment, center of the sample holder was set at the bore axis. However, the bend occurred because the sample holder has finite volume and the position of the sample was off centered. Indeed, the downward flow from the sample located at the left side of the image bend toward the direction of the bore axis.

3.3 Summary

The *in-situ* optical observation system utilizable in high magnetic fields was developed based on Schlieren technique. The fluid motions of optically transparent solution were successfully observed even in high magnetic field owing to the difference of the reflective index that depends on the concentration of solution. As described above, it was observed that the direction of diamagnetic fluid flow was changed under spatially varied magnetic field. This phenomenon was understood qualitatively by considering the magnetic force acting on the high concentration solution and the surrounding solution.

This experimental observation suggest that the fluid flow can be controlled utilizing the magnetic force without any direct contact with the matter even for materials that shows very small response against magnetic fields such as diamagnetic materials. The magnetism is the property that all materials have, therefore, wide range of materials can be controlled by this way. If the understandings about this phenomenon further deepened, the usage of the magnetic force is expected to be applied for many materials processing as a way of control.

Chapter 4

Effects on flow of conducting fluid

- **Lorentz force effects**
- **Magnetically controlled thermal convection**
- **Differentiated effects of the Lorentz force and the magnetic force**

In this chapter, the effect of high magnetic field on thermal convection in conductive aqueous solutions at ambient temperatures was studied through heat transport measurements combined with shadowgraph technique-based visualization. Since the Lorentz force acted on fluid was the major player for the magnetic control of conducting fluid, the effects of Lorentz force on thermal convection in conductive aqueous solutions were first observed and then confirmed by using diamagnetic and paramagnetic conductive fluids. Then, utilizing this effect of Lorentz force, the magnetic induction and damping of the thermal convection of the conductive fluid were experimentally demonstrated. Moreover, to further study the conductive fluid behavior under high magnetic field, the contribution of the Lorentz force and magnetic force on the thermal convection of conductive fluids was separately evaluated.

4.1 Effects of Lorentz force

4.1.1 Diamagnetic conductive solution

At first, to investigate the effect of Lorentz force on thermal convection of conductive fluid, the aqueous solution of ammonium sulfate, $(NH_4)_2SO_4$, was used as the diamagnetic conductive working fluid. The concentration dependence of the conductivity of ammonium sulfate aqueous solution was referred to the literature [131] and is listed in table 4.1. In most of the present experiments, 25.0 wt% aqueous solution was used. Densities of this solution were 1.136×10^3 kg/m^3 at 25.0°C and 1.133×10^3 kg/m^3 at 28.0°C (measured values). The volume magnetic susceptibilities of this solution were estimated using the mass ratio of solute and water as -9.514×10^{-6} at 25.0°C and -9.499×10^{-6} at 28.0°C. In this estimation, mass magnetic susceptibility of ammonium sulfate was assumed to be constant at the both temperatures.

Table 4.1 Electrical conductivities of ammonium sulfate aqueous solutions.

Concentration (wt%)	5.0	10.0	15.0	20.0	25.0
Conductivity (S/m)	5.74	10.5	14.7	18.5	21.5

The center of the sample fluid layer was fixed at the magnetic field center position (z = 0 mm, r = 0 mm). In this configuration, the magnetic field homogeneity in the sample fluid layer is within 10^{-4} in vertical direction and 0.4% in radial direction.

Firstly, the heat transport across the fluid (25.0 wt% ammonium sulfate solution) layer was evaluated with and without magnetic fields. The relationship of measured ΔT values across the fluid layer against the supplied electric powers is shown in figure 4.1. As seen in figure 4.1, ΔT_c was obviously increased when the sample fluid was placed under the magnetic field of 12.0 T. Averages of six data of ΔT_c were 1.72 K for 0.0 T and 2.71 K for 12.0 T, respectively. This means that the thermal convection in conductive aqueous solution was suppressed and that the onset temperature of convection became higher by 1 K under 12.0 T.

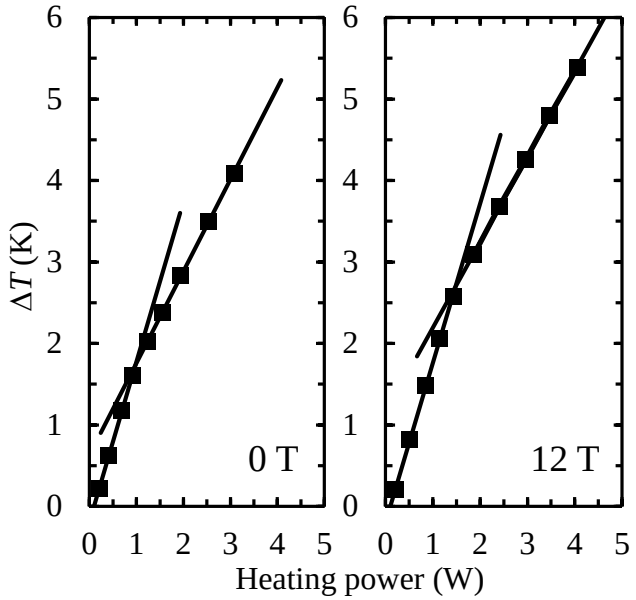

Figure 4.1 Temperature difference across the fluid layer, ΔT, versus the electric power generated by the bottom heater. The concentration of the sample solution is 25.0 wt%. The left and the right sides of the figure indicate the result for 0.0 and 12.0 T. Solid lines were fitted with the least squares method.

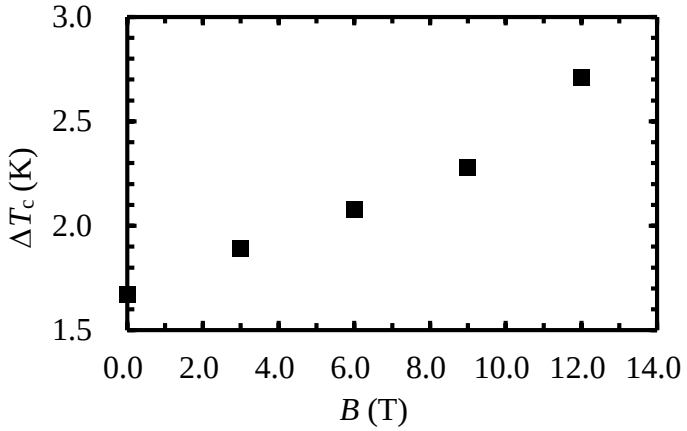

Figure 4.2 Critical temperature difference, ΔT_c, versus the intensity of applied magnetic field, B. The concentration of the sample solution is 25.0 wt%.

Secondly, the dependence of this suppression of convection on the applied magnetic field intensity was evaluated and shown in figure 4.2. The concentration of the solution was also 25.0 wt% in these experiments. The value of ΔT_c monotonically increased with increasing the applied magnetic field. This suppression of convection was also confirmed by visualization experiments and shown in figure 4.3. The shadowgraph images were taken in the neighborhood of the onset of convection under 0.0 (a), 6.0 (b), and 12.0 T (c), respectively. In each case, similar roll patterns appeared when ΔT became sufficiently large and convection occurred, because of the refractive index difference between hot upward flow and cold downward flow. The convection patterns appeared in larger ΔT with increasing magnetic field. This result is consistent with the heat transport measurements. It should be noted that the value of ΔT at the onset was larger than that in the heat conduction experiment. This seems to be due to the different position of the thermocouples and the different thermal conductivities of sapphire

and aluminum bottom plates.

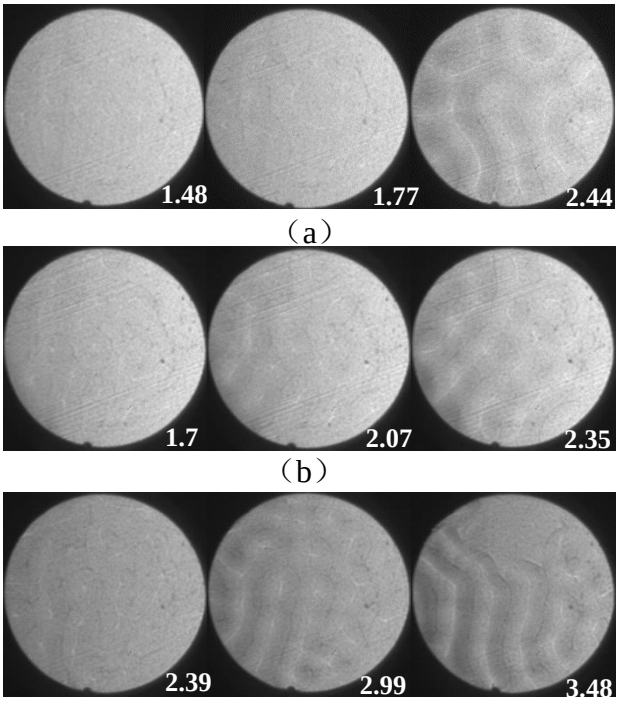

Figure 4.3. Shadowgraph images taken near the onset of convection: (a) 0.0, (b) 6.0, and (c) 12.0 T. The number in each image is the value of ΔT (K) across the fluid layer. The concentration of the sample solution is 25.0 wt%.

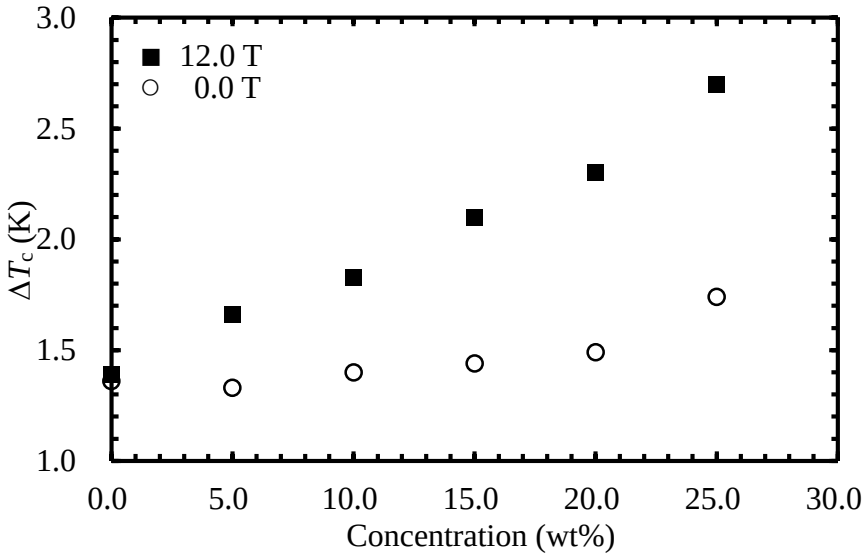

Figure 4.4 Critical temperature difference, ΔT_c, versus the concentration of the solution for 0.0 and 12.0 T.

Thirdly, the dependence of this suppression effect on the concentration of fluid was evaluated by the heat transport measurement. Critical temperature differences, ΔT_c, at 0.0 to 12.0 T were shown for each concentration in figure 4.4. It is clearly seen that the difference of ΔT_c between 0.0 and 12.0

T become larger with increasing the concentration of solution.

4.1.2 Paramagnetic conductive solution

To confirm the suppression effects of magnetic field on thermal convection, 10.0, 15.0 and 20.0 wt% copper nitrate aqueous solutions were used as paramagnetic conductive working fluid. Densities of each solution were measured as 1.081×10^3, 1.131×10^3 and 1.187×10^3 kg/m^3, respectively. Volume magnetic susceptibilities were therefore estimated as 1.295×10^{-6}, 7.144×10^{-6} and 1.357×10^{-5}, respectively. The conductivity of 10.0, 15.0 and 20.0 wt% copper nitrate aqueous solutions in 15.0°C were estimated from literatures [132] as 6.6 S/m, 8.8 S/m and 10.2 S/m, respectively.

Due to the reactivity of copper nitrate aqueous solution against Aluminium, the sapphire bottom plate was used for heat transfer measurement experiments using copper nitrate aqueous solutions. The paramagnetic conductive sample fluids was also fixed at magnetic field center.

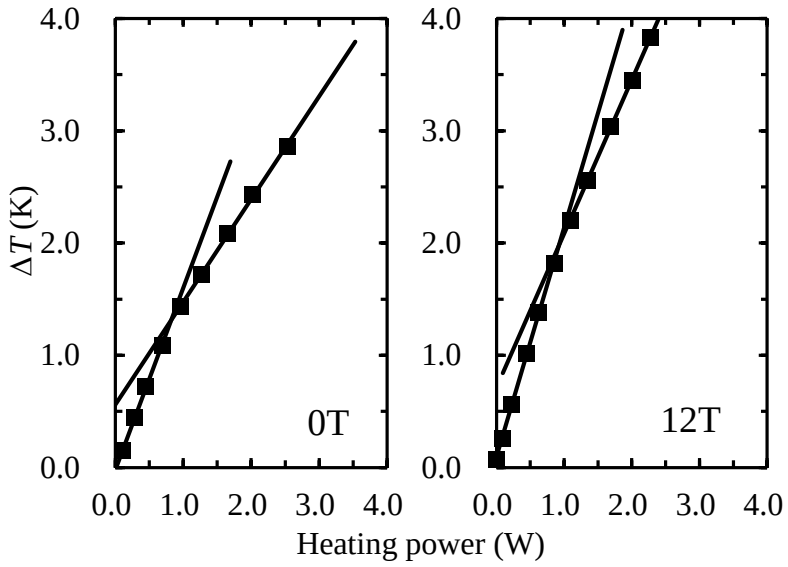

Figure 4.5 Temperature difference across the fluid layer, ΔT, versus the electric power supplied to the bottom heater. The working fluid was 20.0 wt% copper nitrate solution. The left and the right sides of the figure indicate the result for 0.0 T and 12.0 T. Solid lines were fitted with the least squares method.

Figure 4.5 shows the measured temperature difference across the fluid layer (20.0 wt% copper nitrate solution) against the electric power supplied to the bottom heater with and without magnetic fields. As seen in figure 4.4, ΔT_c was obviously increased when the sample fluid was placed under the magnetic field of 12.0 T. Thus obtained ΔT_c values were 1.31 K for 0.0 T and 1.97 K for 12.0 T, respectively. That means the thermal convection in paramagnetic conductive solution was also suppressed under 12.0 T magnetic field.

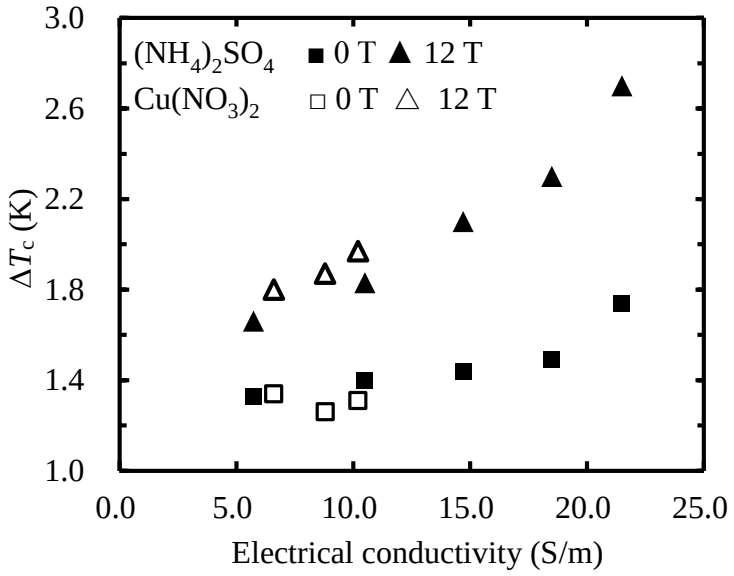

Figure 4.6 Values of ΔT_c were plotted against electrical conductivity of sample solutions. The working fluids were copper nitrate solutions with concentration from 10.0 wt% to 20.0 wt% and ammonium sulfate solutions with concentration from 5.0 wt% to 25.0 wt%.

Then, the dependence of suppression effect on the concentration of solution was evaluated. In this experiment, copper nitrate aqueous solutions of 10.0, 15.0, and 20.0 wt% were used. As described above, both of the paramagnetic susceptibility and the electrical conductivity of solutions increase with increasing the concentration. In the experiment, it was observed that the difference of ΔT_c between 0.0 T and 12.0 T become large depending on the concentration. In figure 4.6, measured ΔT_c at 0.0 T and 12.0 T were plotted against the electrical conductivity of the solution. Results obtained for diamagnetic ammonium sulfate aqueous solutions with concentration from 5.0 wt% to 25.0 wt% in the previous experiment were also showed in the figure. As seen in the figure 4.6, the suppression of thermal convection became larger with increasing the electrical conductivity for both of the sample fluids regardless of their magnetism.

4.1.3 The origin of suppression effects

The origin of the suppression of thermal convection in conductive fluid under high magnetic fields seems to be a dynamical effect due to magnetically induced forces. Within the conditions of the present study, these forces may be related to either the magnetic force acting on materials under the gradient magnetic fields or the Lorentz force due to the induced electric current in the fluid when the conductive fluid moves in the magnetic field.

It is well known that thermal convection in a feeble magnetic fluid is affected by large magnetic force due to high gradient magnetic field. Across a superconducting magnet bore, magnetic field is not quite uniform in general and magnetic field gradient, *dB/dz*, exists. The estimated $B \cdot dB/dz$ in the present sample space is around ±12.0 T^2/m, and the maximum magnetic force acting on the diamagnetic sample fluid in this case is about 90 N/m^3. The thermal convection is induced due to the difference of the gravitational force acting on fluids between the top and the bottom that caused by

the temperature difference. The contribution of the magnetic force on the thermal convection can be estimated by considering the relative ratio of the magnetic force against the gravitational force acting on the fluid. For 25.0 wt% diamagnetic ammonium sulfate aqueous solution, the gravitational force per unit volume acting on the fluid is about 1.11×10^{4} N/m^3. Therefore, the contribution of the magnetic force seems to be only 1% or less. In an earlier study that reported the suppression and the enhancement of the thermal convection of water, the sample fluid was placed under high and steep magnetic field such as $B\cdot dB/dz = \pm417$ T^2/m, and the contribution of the magnetic force turned out to be 30% of the gravitational force. [71]

Furthermore, the heat transport measurements were also carried out using the paramagnetic aqueous solution. Under the same magnetic field environment, directions of the magnetic force acting on paramagnetic fluids and diamagnetic fluids are opposite. It has been reported that the thermal convection in paramagnetic and diamagnetic fluid can be either suppressed by upward magnetic force (anti-parallel to the gravity force) or enhanced by downward magnetic force (parallel to the gravity force). [44,71] In the present study, as the case of the diamagnetic fluid, the thermal convection was suppressed also in the paramagnetic fluid, therefore, it was experimentally confirmed that the suppression of the thermal convection of conductive fluids under the magnetic field observed here was not caused by the magnetic force.

We now consider the contribution of the Lorentz force. It is experimentally known that the velocity of the thermal convection, v, is given by

$$v = {}^{h}/_{(c_p \cdot \rho_0)} \tag{4.1}$$

where h is the average heat transfer coefficient, c_p is the thermal capacity of the fluid, and ρ_0 is the average density of the fluid. [133] In the present experimental setup, the velocity of the thermal convection of water is estimated to be about 67×10^{-6} m/s when the temperature difference between the top and the bottom of the convection cell is 3 K. If all of the ammonium sulfate dissolved in the solution are ionized and have this velocity, the intensity of the Lorentz force can be estimated as 6.7×10^{5} N/m^3 from an equation,

$$F_L = qvB \tag{4.2}$$

Since ammonium sulfate is not a salt from strong acid and strong base, its ionization does not proceed a lot. Assuming the degree of ionization is several percent, the intensity of the Lorentz force will be same order with that of the gravitational force. The Lorentz force acts on the conductive fluid so as to hinder the fluid flow. Therefore, it is reasonable to believe that the suppression of the thermal convection of conductive diamagnetic fluid under the magnetic field observed here was caused by the Lorentz force.

4.2 Magnetically controlled thermal convection

4.2.1 Suppression

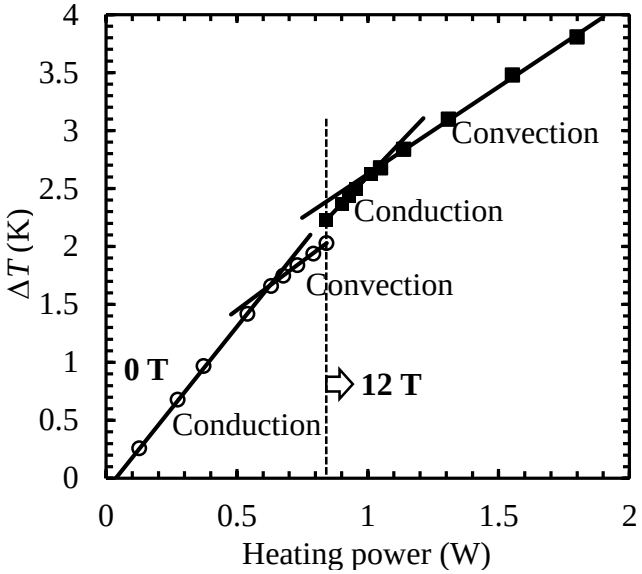

Figure 4.7 Damping of the thermal convection caused by the application of magnetic field. The ΔT is plotted against the electric power generated by the bottom heater. Solid line fitting is based on the least squares method.

We now tried to demonstrate the magnetic field control of the thermal convection of conductive fluid using the present experimental setup. The sample solution used here was 25.0 wt% diamagnetic ammonium sulfate aqueous solution and the experimental results are shown in figure 4.7.

In the experiment without magnetic field, the heating power supplied to the bottom heater was first increased until the onset of convection was observed. Then, the heating power was kept at a constant value, as indicated in the figure with a dashed line, and the magnetic field up to 12.0 T was applied. At this stage ΔT increased gradually with increasing magnetic field. After the applied magnetic field reached 12.0 T, the heating power was again increased. As seen in the figure, the increasing rate of ΔT became larger. This means that the convection was damped and the heat transport was dominated by the conduction. With further increase of the heating power, the onset of the convection was observed again.

4.2.2 Induction

We carried out a backward experiment and the results are shown in figure 4.8. The sample solution used here was also 25.0 wt% diamagnetic ammonium sulfate aqueous solution. The heater power was first increased at 12.0 T and kept at a constant value when the value of ΔT became around 2.15 K; larger than ΔT_c at 0.0 T (1.72 K on average) and smaller than that at 12.0 T (2.71 K). For these heater

power and ΔT, the heat transport was still dominated by the conduction. Then, the magnetic field was gradually decreased to 0.0 T. The change of ΔT during this process was shown in the inset of figure 4.8. At the beginning, ΔT did not change appreciably with deceasing magnetic field. However, the magnetic field fell below a certain value, ΔT rapidly decreased. This is due to the convection induced by decreasing magnetic field. The heater power was increased again, when the magnetic field came down to 0.0 T. As seen in the figure, the increasing rate of ΔT was gradual as the convection state. These have clearly demonstrated that the heat transport in a conductive aqueous solution can be controlled by the application of magnetic fields.

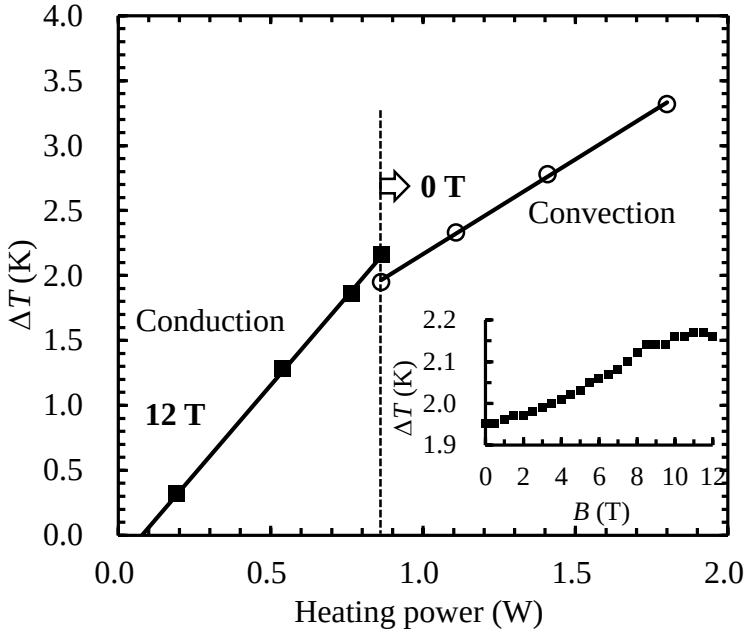

Figure 4.8 Induction of the thermal convection by decreasing the magnetic field. The ΔT is plotted against the electric power generated by the bottom heater. Solid line fitting is based on the least squares method. The inset shows the change of temperature difference, ΔT, during this process.

4.3 Differentiated effects of the Lorentz force and the magnetic force

When the sample fluid with finite volume was fixed under magnetic field generated by a superconducting magnet, the magnetic force seems unavoidable due to the magnetic field gradient. That means, for the conductive fluid in magnetic field, the effect of Lorentz force was always accompanied with a certain extent of magnetic force effect. It seems necessary to distinguish the effects of Lorentz force and magnetic force on conductive fluid behavior.

4.3.1 Magnetic field condition

In order to distinguish the effects of the magnetic force and the Lorentz force, one of the magnetic field conditions, $B \cdot dB/dz$ or B, was fixed at constant value and the other was varied in a series of experiments. As is well-known, the intensity of the magnetic force depends on value of $B \cdot dB/dz$ while the Lorentz force depends on the intensity of the magnetic field. In this series of experiments, 25.0

wt% diamagnetic ammonium sulfate aqueous solution was used. Sample fluid was fixed at several different positions in the magnet bore. Locations along the bore axis and magnetic field conditions used in present study are listed in tables 4.2 and 4.3. In case of experiments described in table 4.2, the magnetic field at the center of the sample fluid was fixed at 9.0 T and $B \cdot dB/dz$ values were changed from -549 to +549 T^2/m. In experiments described in table 4.3, $B \cdot dB/dz$ values were fixed at around -360, 0, +360 T^2/m, applied magnetic fields were changed from 5.5 to 12.0 T.

Table 4.2 Locations along the bore axis and magnetic field conditions of working fluids in experiments with fixed value of B and changed value of $B \cdot dB/dz$.

z (mm)	B at sample center (T)	$B \cdot dB/dz$ (T^2/m)	B at magnetic field center (T)
106	9.0	-549	12.0
82	9.0	-362	10.5
51	9.0	-185	9.5
0	9.0	0	9.0
-51	9.0	185	9.5
-82	9.0	362	10.5
-106	9.0	549	12.0

4.3.2 Results and discussion

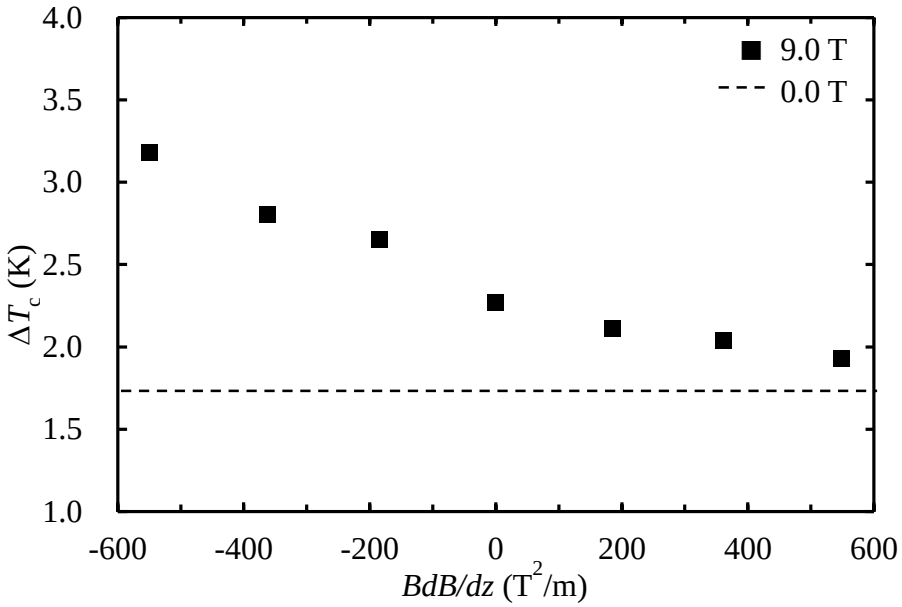

Figure 4.9 The relationship of measured ΔT_c value against the value of $B \cdot dB/dz$, when magnetic field intensities were fixed at 9.0 T. The working fluid was 25wt% ammonium sulfate aqueous solution. The dashed line indicates the ΔT_c value of sample fluid obtained without magnetic field.

Figure 4.9 shows the relationship of measured ΔT_c against the value of $B \cdot dB/dz$ when the applied

magnetic field in the center of the sample fluid was fixed at 9.0 T. The magnetic field condition was illustrated in table 4.2. The dashed line indicates the ΔT_c value obtained without magnetic field, which is 1.72 K by average of six data. As seen in the figure, when intensity of magnetic fields was fixed, obtained ΔT_c value changed systematically depending on the value of $B \cdot dB/dz$. The direction of the magnetic force acting on a diamagnetic fluid is vertically upward when $B \cdot dB/dz$ is negative and downward when $B \cdot dB/dz$ is positive. The upward force contributes to suppress the thermal convection, and the downward force contributes to enhance it, however, the thermal convection was suppressed compared with the case of 0.0 T in all positions as a result of the superposition effect due to the Lorentz force.

Table 4.3 Locations along the bore axis and magnetic field conditions of working fluids in experiments with fixed value of $B \cdot dB/dz$ and changed value of B.

z (mm)	B at sample center (T)	$B \cdot dB/dz$ (T^2/m)	B at magnetic field center (T)
±157	5.5	∓360	12.0
±129	6.2	∓363	10.0
±92	8.2	∓360	10.0
±76	9.7	∓364	11.0
±62	11.0	∓365	12.0
0	6.0	0	6.0
0	9.0	0	9.0
0	12.0	0	12.0

Figure 4.10 shows the relationship of measured ΔT_c against the value of B at the center of the fluid when $B \cdot dB/dz$ values were fixed at around -360, 0, +360 T^2/m, respectively. In this series of experiments, intensities of magnetic fields were changed from 5.5 to 12.0 T. The magnetic field condition was illustrated in Table 4.3. The solid lines are the best fits by the least square method. The dashed line indicates the ΔT_c value of sample fluid obtained without magnetic field as shown in figure 4.9. In case of any $B \cdot dB/dz$ value, the suppression effect of thermal convection became larger with increasing applied magnetic fields. With considering the direction of the magnetic force acting on the fluid, it is consistent with the result shown in figure 4.9 that the suppression effect became larger and smaller when $B \cdot dB/dz$ is negative and positive compared with the case of 0.0 T, respectively. The slopes of fitted lines are similar. This means that the dependence of ΔT_c on magnetic field intensity is similar when the value of $B \cdot dB/dz$ is changed.

These features of the result can be understood by considering the superposition of the Lorentz force due to the induced electric current in the fluid when the conductive fluid moves in the magnetic field and the magnetic force acting on materials under the gradient magnetic fields. In case of the experiment in figure 4.9, the suppression effect by the Lorentz force was constant because of the fixed applied magnetic field and the contribution of the magnetic force varied with the variation of $B \cdot dB/dz$. On the other hand, in case of the experiment in figure 4.10, the effect of the magnetic force was constant because the value of $B \cdot dB/dz$ was fixed and the contribution of the Lorentz force varied due to the change of the applied magnetic field. As seen in figure 4.10, when the applied magnetic field

was 6.2 T and $B \cdot dB/dz$ was 360 T^2/m, the value of ΔT_c is almost same with the case of 0.0 T. In this case, the contribution of both forces seemed balanced with each other.

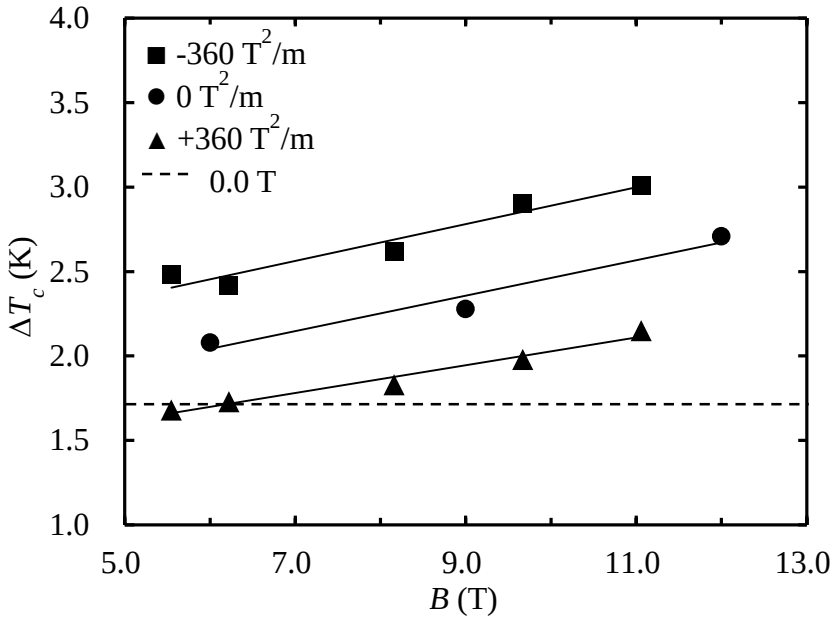

Figure 4.10 The relationship of measured ΔT_c value against the value of B at the center of the fluid when the values of $B \cdot dB/dz$ were fixed at around -360, 0, +360 T^2/m, respectively. The working fluid was 25.0 wt% ammonium sulfate aqueous solution. Solid lines were fitted with the least squares method. The dashed line indicates the ΔT_c value of sample fluid obtained without magnetic field.

To further understand this superposition effect, we assume that the intensity of magnetic force and the Lorentz force acted on fluid was equal under magnetic field condition that B was 6.2 T and $B \cdot dB/dz$ was 360 T^2/m. Based on the calculation mentioned previous, the velocity of the thermal convection of water was estimated to be about 67×10^{-6} m/s when the temperature difference between the top and the bottom of the convection cell was 3 K. The magnetic force in this case was calculated as 2.7×10^3 N/m^3 based on the equation (1.1). Then the ionization rate of 25.0 wt% ammonium sulfate aqueous solution was estimated as 0.79% based on equation (4.2). Thus the intensity of magnetic force and Lorentz force can be both evaluated under each condition in figure 4.10. As result, the contributions of the Lorentz force and the magnetic force on effect of magnetic field in the figure 4.10 can be estimated as percentages. For example, both forces contribute to the suppression of thermal convection in negative gradient magnetic field, the contribution of Lorentz force increased from 47.11% to 63.73% when the value of B changed from 5.5 T to 11.0 T. For another, in positive gradient magnetic field, the downward magnetic force contributes to enhance the thermal convection while the Lorentz force still contributes to suppress it. When the value of B on the fluid was 5.5 T, 89.09% of the magnetic force was balanced by Lorentz force, hence the thermal convection was slightly enhanced compared with the case of 0.0 T; while the 11.0 T magnetic field was applied, the magnetic force was only 56.94% that of Lorentz force, the thermal convection was therefore effectively suppressed.

4.4 Summary

Heat transport measurements and visualization of thermal convection in conductive aqueous solutions were carried out in high magnetic fields. Under the magnetic fields up to 12.0 T, the thermal convection in conductive solution was suppressed. The magnitude of this suppression effect depends on the applied magnetic field and the concentration of the fluid. Through the comparison of magnetic field effects on diamagnetic and paramagnetic conductive fluid, it was found that the magnitude of this suppression effect depends on the electrical conductivity of sample fluids regardless of their magnetism. This suppression of the thermal convection of conductive fluids under the magnetic field was therefore experimentally confirmed as the effect of the Lorentz force.

The magnetic induction and damping of the thermal convection of the conductive fluid were experimentally demonstrated. Furthermore, the contribution of the Lorentz force and magnetic force on the thermal convection of feeble magnetic conductive fluids was separately evaluated by changing the magnetic field environment. These results show that the effect of the Lorentz force and the magnetic force can be investigated individually by using electrolytes aqueous solution combined with a superconducting magnet. The results obtained should help us to deepen the understanding of conductive fluid behavior in magnetic fields.

Chapter 5

Conclusion and outlook

5.1 Conclusion

As described in chapter 1, the magnetic control of fluid flow has become an important means to improve the quality of material, but still has some limitations in practical industry processing. The objective of the thesis is to improve the magnetic control of fluid flow by addressing the experimental observation of feeble magnetic fluid flow under high magnetic fields.

Results of the research done for this thesis are summed up as follows.

Effects of high magnetic field on non-conductive fluid flow

The *in-situ* optical observation system utilizable in high magnetic fields was developed based on Schlieren technique. The fluid motions of optically transparent solution were successfully observed even in high magnetic field owing to the difference of the reflective index that depends on the concentration of solution. It was observed that the direction of diamagnetic non-conducting fluid flow was changed under spatially varied magnetic field. This phenomenon was understood qualitatively by considering the magnetic force acting on the high concentration solution and the surrounding solution.

Effects of high magnetic field on conductive fluid flow

Under the magnetic fields up to 12.0 T, the thermal convection in conductive solution was suppressed. The magnitude of this suppression effect depends on the applied magnetic field and the concentration of the fluid. Through the comparison of magnetic field effects on diamagnetic and paramagnetic conductive fluid, it was found that the magnitude of this suppression effect depends on the electrical conductivity of sample fluids regardless of their magnetism. This suppression of the thermal convection of conductive fluids under the magnetic field was therefore experimentally confirmed as the effect of the Lorentz force.

The magnetic induction and damping of the thermal convection of the conductive fluid were experimentally demonstrated. Furthermore, the contribution of the Lorentz force and magnetic force on the thermal convection of feeble magnetic conductive fluids was separately evaluated by changing the magnetic field environment. These results show that the effect of the Lorentz force and the magnetic force can be investigated individually by using electrolytes aqueous solution combined with a superconducting magnet.

5.2 Outlook

Through the experimental observation in this thesis, the behavior of fluid flow under high magnetic fields was intuitively observed by self-built *in-situ* optical observation system. Effects of the Lorentz force and the magnetic force on convection in non-conductive and conductive fluids were both observed and quantitatively understood. Owing to these works, the understanding of feeble magnetic fluid behavior under high magnetic fields was deepened.

For the optimization of magnetic control processing in melting metal, the intuitive experimental observation is significant but still lacking owing to the high temperature and low light transparency

of liquid metal. However, the study in this thesis shows that it seems feasible to understand the behaviors of liquid metals by using electrolytes aqueous solution combined with a superconducting magnet since flow conditions thereby are regarded as similar to those for liquid metals in industrial electromagnets. Use of aqueous solutions enables us experiments under room temperature and also expected to bring spatial information about the convection in a fluid since they have optical transparency in many case.

Therefore, utilizing this technique, more valuable experimental evidences can be provided to confirm the numerical simulation in industry processing. Once the model used in numerical simulation is proved appropriate, valued information can be obtained for optimization of the magnetic control processing.

References

1) O. G. Martynenko, P. P. Khramtsov, Free-convective heat transfer, Springer Science and Business Media, Berlin, 2005.

2) A. Y. Gelfgat, P. Z. Bar-Yoseph and A. Solan, Effect of axial magnetic field on three-dimensional instability of natural convection in a vertical Bridgman growth configuration, J. Cryst. Growth 230, 63 (2001).

3) C. Karcher, Y. Kolesnikov, O. Andreev and A. Thess, Natural convection in a liquid metal heated from above and influenced by a magnetic field, Eur. J. Mech. B 21, 75 (2002).

4) G. Muller, Convection and inhomogeneities in crystal growth from the melt, Springer, Berlin, 143, 1986 (1988).

5) I. A. Prokhorov, Y. A. Serebryakov, B. G. Zakharov, I. Z. Bezbakh, V. V. Ratnikov, I. L. Shulpina, Growth striations and dislocations in highly doped semiconductor single crystals, J. Cryst. Growth 310, 5477 (2008).

6) M. C. Schneider, J. Gu, C. Beckermann, Segregation in directional solidification of superalloys, solidification laboratory, University of Iowa, Feb. 17th 2004, http://user.engineering.uiowa.edu/~becker/3dfreckle.htm

7) M. R. Mackley, A. Keller, Flow induced polymer chain extension and its relationship to fibrous crystallization, Phil. Trans. Royal Soc. 278, 29 (1975).

8) V. Metan, K. Eigenfeld, D. Räbiger, M. Leonhardt, S. Eckert, Grain size control in Al–Si alloys by grain refinement and electromagnetic stirring, J. Alloys. Compd. 487, 163 (2009)

9) F. Otalora, M. L. Novella, J. A. Gavira, B. R. Thomas, J. M. Garcia-Ruiz, Experimental evidence for the stability of the depletion zone around a growing protein crystal under microgravity, Acta Cryst D57, 412 (2001).

10) A. McPherson, Crystallization of biological macromolecules, Cold Spring Harbor Lab. Press, 1999.

11) F. Otalora, M. Luisa, et al., Experimental evidence for the stability of the depletion zone around a growing protein crystal under microgravity, Acta Cryst. D57, 412 (2001).

12) C. E. Kundrot, R. A. Judge, M. L. Pusey, E. H. Snell, Microgravity and macromolecular crystallography, Cryst. Growth Des. 1 87 (2001).

13) B. Billia, H. Jamgotchian, J. I. Favier, D. Camel, Proceedings of the norderney symposium on scientific results of the German spacelab mission Dl, P. R. Sahm, R. Jansen, M. H. Keller (Eds.), Koln: WPF, 230 (1987).

14) B. Zhou, Y. L. Kang, J. Zhang, J. Z. Gao, F. Zhang. Forced convection rheomoulding process for semisolid slurry preparation and microstructure evolution of 7075 aluminum alloy, Solid State Phenomena 192, 422 (2013).

15) B. Zhou, Y. L. Kang, G. M. Zhu J. Z. Gao, M. F. Qi, Forced convection rheoforming process for preparation of 7075 aluminum alloy semisolid slurry and its numerical simulation, Trans. Nonferrous Met. Soc. China 24, 1109 (2014).

16) J. Friedrich, J. Baumgartl, H.J. Leister, G. Müller, Experimental and theoretical analysis of convection and segregation in vertical Bridgman growth under high gravity on a centrifuge, J. Cryst. Growth 167, 45 (1996).

17) L. L. Rodot, M. Rodot, W. R. Wilcox, Material processing in high gravity-proceedings of the 1st international workshop on material processing in high gravity, J. Cryst. Growth R8, 119 (1992).

18) C. W. Lan, C. H. Chian, Three-dimensional simulation of Marangoni convection in floating-zone crystal growth, J. Cryst. Growth 230, 172 (2001).

19) S. Eckert, P. A. Nikrityuk, B. Willers, D. Räbiger, N. Shevchenko, H. Neumann-Heyme, V. Travnikov, S. Odenbach, A. Voigt, K. Eckert, Electromagnetic melt flow control during solidification of metallic alloys, Eur. Phys. J. Special Topics 220, 123 (2013).

20) R. W. Series and D. T. J. Hurle, The use of magnetic fields in semiconductor crystal growth, J. Cryst. Growth 113, 305 (1991).

21) E. Beaugnon, D. Bourgault, D. Braithwaite, P. De Rango, R. Perrier De La Bathie, Andre Sulpice, R. Tournier, Material processing in high static magnetic field. A review of an experimental study on levitation, phase separation, convection and texturation, J. Phys. I France 3, 399 (1993).

22) H. Yasuda, T. Toh, K. Iwai, K. Morita, Recent progress of EPM in steelmaking, casting, and solidification processing, ISIJ Int. 47, 619 (2007).

23) M. Watanabe, M. Eguchi and T. Hibiya, Silicon crystal growth by the electromagnetic Czochralski (EMCZ) method, Jpn. J. Appl. Phys. 38, 10 (1999).

24) L. D. Landau and E. M. Lifshitz, Electrodynamics of Continuous Media, Pergamon Press, Oxford, 1960.

25) M. Yamaguchi, Y.Tanimoto, Magneto-science, Kodansha and Springer, Berlin, 2006.

26) D. A. Watring, S. L. Lehoczky, Magneto-hydrodynamic damping of convection during vertical Bridgman–Stockbarger growth of HgCdTe, J. Cryst. Growth 167, 478 (1996).

27) R. Aogaki, K. Fueki, T. Mukaibo, Application of magnetohydrodynamic effect on the analysis of electrochemical reactions, MHD flow of an electrolyte solution in an electrode-cell with a short rectangular channel, Denki Kagaku 43, 504 (1975).

28) I. Mogi, S. Okubo, Y. Nakagawa, Dense radial growth of silver metal leaves in a high magnetic field, J. Phys. Soc. Jpn. 60, 3200 (1991).

29) S. Chandrasekhar, Hydrodynamic and hydromagnetic stability, Dover Publications, New York, 1981.

30) Y. Ito, Kagaku to kyoiku (Chemistry and Education), The chemical society of Japan, 38, 86 (1990).

31) M. Fujiwara, D. Kodoi, W. Duan, Y. Tanimoto, Separation of transition metal ions in an inhomogeneous magnetic field, J. Phys. Chem. B 105, 3343 (2001).

32) T. Ohara, S.Mori, Y. Oda, Y. Wada, O. Tsukamoto, Feasibility of magnetic chromatography for ultra-fine particle separation, Tans. IEE of Japan 116B-8, 979 (1996).

33) E. Beaugnon, R. Tournier, Levitation of organic materials, Nature 349, 470 (1991).

34) K. Kitazawa, Y. Ikezoe, H. Uetake, N. Hirota, Magnetic field effects on water, air and powders, Physica B 294, 709 (2001).

35) M. Iwasaka, S. Ueno, Properties of diamagnetic fluid in high gradient magnetic fields, J. Appl. Phys. 75-10, 7177 (1994).

36) N. Hirota, T. Homma, H. Sugawara, K. Kitazawa, M. Iwasaka, S. Ueno, H. Yokoi, Y. Kakudate, S. Fujiwara and M. Kawamura, Rise and fall of surface level of water solutions under high magnetic field, Jpn. J. Appl. Phys. 34, L991 (1995).

37) Y. Ikezoe, N. Hirota, J. Nakagawa, K. Kitazawa, Making water levitate, Nature 393,749 (1998).

38) T. de L. Etienne du, G. Damien and S. Michel, Magnetism, Springer since and Business media, Boston, 2005.

39) T. Albrecht, C. Bührer, M. Fähnle, K. Maier, D. Platzek, J. Reske, First observation of ferromagnetism and ferromagnetic domains in a liquid metal, Applied Physics A 65-2, 215 (1997).

40) G. Sazaki, Crystal quality enhancement by magnetic fields, Prog. Biophys. Mol. Biol. 101, 45 (2009).

41) Q. Wang, T. Liu, K. Wang, P. F. Gao, Y. Liu and J. C. He, Progress on high magnetic field-controlled transport phenomena and their effects on solidification microstructure, ISIJ Int. 54-3, 516 (2014).

42) J. R. Carruthers, R. Wolfe, Magnetothermal convection in insulating paramagnetic fluids, J. Appl. Phys. 39, 5718 (1968).

43) Z. H. I. Sun, M. Guo, J. Vleugels, O. Van der Biest, B. Blanpain, Processing of non-ferromagnetic materials in strong static magnetic field, Curr. Opin. Solid State Mater. Sci. 17-4, 193 (2013)

44) D. Braithwaite, E. Beaugnon and R. Tournier, Magnetically controlled convection in a paramagnetic fluid, Nature 134, 354 (1991).

45) H. Uetake, N. Hirota, J. Nakagawa, Y. Ikezoe and K. Kitazawa, Thermal convection control by gradient magnetic field, J. Appl. Phys. 87, 6310 (2000).

46) L. Pleskacz, E. Fornalik-Wajs, Magnetic field impact on the high and low Reynolds number flows, J. Phys.: Conf. Ser. 50, 012062 (2014).

47) P. W. G. Poodt, P. C. M. Christianen, W. J. P. van Enckevort, J. C. Maan, E. Vlieg, The critical Rayleigh number in low gravity crystal growth from solution, Cryst. Growth Des. 8, 2194 (2008).

48) J. Huang, D. D. Gray, Thermoconvective instability of paramagnetic fluids in a nonuniform magnetic field, Phys. Rev. E 57-5, 5564 (1998).

49) J. Huang, B. F. Edwards, D. D. Gray, Magnetic control of convection in nonconducting paramagnetic fluids, Phys. Rev. E 57-1, 29 (1998).

50) T. Tagawa, R. Shigemitsu, H. Ozoe, Magnetizing force modeled and numerically solved for natural convection of air in a cubic enclosure: effect of the direction of the magnetic field, Int. J. Heat Mass Transfer 45, 267 (2002).

51) E. Fornalik, P. Filar, T. Tagawa, H. Ozoe, J. S. Szmyd, Experimental study on the magnetic convection in a vertical cylinder, Exp. Therm Fluid Sci. 29, 971 (2005).

52) E. Fornalik, P. Filar, T. Tagawa, H. Ozoe, J. S. Szmyd, Effect of a magnetic field on the convection of paramagnetic fluid in unstable and stable thermosyphon-like configurations, Int. J. Heat Mass Transfer 49, 2642 (2006).

53) W. A. Wrobel, E. Fornalik-Wajs, J. S. Szmyd, Experimental and numerical analysis of thermo-magnetic convection in a vertical annular enclosure, Int. J. Heat Fluid Flow 31, 1019 (2010).

54) W. A. Wrobel, E. Fornalik-Wajs, J. S. Szmyd, Analysis of the influence of a strong magnetic field gradient on convection process of paramagnetic fluid in the annulus between horizontal concentric cylinders, J. Phys.: Conf. Ser. 395, 012124 (2012).

55) P. W. G. Poodt, M. C. R. Heijna, K. Tsukamoto, W. J. D. Grip, P. C. M. Christianen, J. C. Maan, W. J. P. van Enckevort, E. Vlieg,. Suppression of convection using gradient magnetic fields during crystal growth of $NiSO_4$ center dot 6H(2)O, Appl. Phys. Lett. 87, 214105 (2005).

56) P. W. G. Poodt, M. C. R. Heijna, P. C. M. Christianen, W. J. P. van Enckevort, W. J. D. Grip, K. Tsukamoto, J. C. Maan, E. Vlieg,. Using gradient magnetic fields to suppress convection during crystal growth, Cryst. Growth Des. 6, 2275 (2006).

57) M. C. R. Heijna, P. W. G. Poodt, K. Tsukamoto, W. J. D. Grip, P. C. M. Christianen, J. C. Maan, J. L. A. Hendrix, W. J. P. van Enckevort, E. Vlieg, Magnetically controlled gravity for protein crystal growth, Appl. Phys. Lett. 90, 264105 (2007).

58) P. W. G. Poodt, M. C. R. Heijna, P. C. M. Christianen, W. J. P. van Enckevort, J. C. Maan, E. Vlieg,. A comparison between simulations and experiments for microgravity crystal growth in gradient magnetic fields, Cryst. Growth Des. 8-b, 2200 (2008).

59) J. Huang, D. D. Gray and B. F. Edwards, Magnetic control of convection in nonconducting diamagnetic fluids, Phys. Rev. E 58, 5164 (1998).

60) J. W. Qi, N. I. Wakayama, A. Yabe. Attenuation of natural convection by magnetic force in electro-nonconducting fluids. J. Cryst. Growth 204, 408 (1999).

61) T. Tagawa, A. Ujihara and H. Ozoe, Numerical computation for Rayleigh-Benard convection of water in a magnetic field, Int. J. Heat Mass Transf. 46, 4097 (2003).

62) S. Maki, M. Ataka, Suppression and promotion of convection in water by use of radial components of the magnetization force, J. Appl. Phys. 96, 1696 (2004).

63) S. Maki, M. Ataka, Three-dimensional computation of convection of water at the center of a superconducting magnet, Phys. Fluids 17, 087107 (2005).

64) J. W. Qi, N. I. Wakayama, Suppression of natural convection in nonconducting and lowconducting fluids by the application of a static magnetic field, Mater. Trans., JIM 41, 970 (2000).

65) N. I. Wakayama, Effects of a strong magnetic field on protein crystal growth, Cryst. Growth Des. 3-1, 17 (2003).

66) N. I. Wakayama, Damping of solute convection during crystal growth by applying magnetic field gradients, Jpn. J. Appl. Phys. Part 2 44, L833 (2005).

67) J. W. Qi, N. I. Wakayama, The combined effects of magnetic field and magnetic field gradients on convection in crystal growth, Phys. Fluids 16, 3450 (2004).

68) J. W. Qi, N. I. Wakayama, M. Ataka, Magnetic suppression of convection in protein crystal growth processes, J. Cryst. Growth 232, 132 (2001).

69) L. B. Wang, N. I. Wakayama, Effects of strongmagnetic fields on natural convection in the vicinity of a growing cubic protein crystal, ISIJ Int. 43, 877 (2003).

70) L. B. Wang, C. W. Zhong, N. I. Wakayama, Damping of natural convection in the aqueous protein solutions by the application of high magnetic fields, J. Cryst. Growth 237, 312 (2002).

71) H. Nakamura, T. Takayama, H. Uetake, N. Hirota and K. Kitazawa, Magnetically controlled convection in a diamagnetic fluids, Phys. Rev. Lett. 94, 144501 (2005).

72) R. Hirose, S. Hayashi, Y. Watanabe, Y. Yokota, M. Takeda, H. Kurahashi, K. Kosaka, K. Shibutani,. Development of a superconducting magnet for high magnetic force field application, IEEE Trans Appl Supercond. 17, 2299 (2007).

73) T. Kiyoshi, O. Ozaki, H. Morita, H. Nakayama, H. B. Jin, H. Wada, N. I. Wakayama, M. Ataka, Superconducting magnets for generating uniform magnetic force field, IEEE Trans Appl Supercond. 9, 362 (1999).

74) O. Ozaki, T. Kiyoshi, S. Matsumoto, K. Koyanagi, J. Fujihira, H. Nakayama, H. Wada, Design study of superconducting magnets for uniform and high magnetic force field generation, IEEE Trans Appl Supercond. 11, 2252 (2001).

75) O. Ozaki, K. Koyanagi, T. Kiyoshi, S. Matsumoto, J. Fujihira, H. Wada, Development of superconducting magnets for uniform and high magnetic force field generation, IEEE Trans Appl Supercond. 12, 940 (2002).

76) L. Quettier, O. Vincent-Viry, A. Mailfert, F. P. Juster, Micro-gravity: superconducting coils for crystal growth. Influence of the levitation force on natural convection in the fluid, Eur. Phys. J.-Appl. Phys 22, 69 (2003).

77) B. A. Finlayson, Convective in stability of ferromagnetic fluids, J. Fluid Mech. 40, 753 (1970).

78) L. Schwab, Konvektion in ferrofluiden, Ludwig-Maximilians-Universität München, Diss, 1989.

79) L. Schwab, U. Hildebrandt, K. Stierstadt, Magnetic Bénard convection, J. Mag. Mag. Mater.39, 113 (1983).

80) S. Odenbach, Microgravity experiments on thermomagnetic convection in magnetic fluids, J. Mag. Mag. Mater.149, 155 (1995).

81) W. Luo, T. Du, J. Huang, Field-induced instabilities in a magnetic fluid, J. Magn. Magn. Mater. 201, 88 (1999).

82) W. Luo, T. Du, J. Huang, Novel convective instabilities in a magnetic fluid, Phys. Rev. Lett. 82-20, 4134 (1999).

83) H. Engler, Parametische modulation thermomagnetischer konvektion in ferrofluiden, Technische Universität Dresden, Diss, 2010.

84) H. Engler, S. Odenbach, Parametric modulation of thermomagnetic convection in magnetic fluids, J. Phys.: Condens. Matter 20, 204135 (2008).

85) H. Engler, A. Lange, D. Borin, S. Odenbach, Hindrance of thermomagnetic convection by the magnetoviscous effect, Int. J. Heat Mass Transf. 60, 499 (2013).

86) M. Heckert, L. Sprenger, A. Lange, S. Odenbach, Experimental determination of the critical Rayleigh number for thermomagnetic convection with focus on fluid composition, J. Magn. Magn. Mater. 381, 337 (2015).

87) B. Huke, M. Lücke, Roll, square, and cross-roll convection in ferrofluids, J. Mag. Mag. Mater. 289, 264 (2005).

88) D. Laroze, P. G. Siddheshwar, H. Pleiner, Chaotic convection in a ferrofluid, Commun. Nonlinear Sci. Numer. Simul. 18, 2436 (2013).

89) B. M. Berkovsky, V. E. Fertman, V. K. Polevikov, S. V. Isaev, Heat transfer across vertical ferrofluid layers, Int. J. Heat Mass Transf. 19, 981 (1976).

90) Z. H. I. Sun, M. Guo, J. Vleugels, O. Van der Biest, B. Blanpain, Strong static magnetic field processing of metallic materials: A review, Curr. Opin. Solid State Mater. Sci. 16, 254 (2012).

91) Q. Wang, T. Liu, K. Wang, C. J. Wang, K. Nakajima and J. C. He, Solidified structure control of metallic materials by static high magnetic fields, ISIJ Int. 50-12, 1941 (2010).

92) S. Chandrasekhar, On the inhibition of convection by a magnetic field 2, Philos. Mag. 45, 1177 (1954).

93) Y. Nakagawa, An experiment on the inhibition of thermal convection by a magnetic field, Nature 175, 417 (1955).

94) K. Jirlow, Experimental investigation of the inhibition of convection by a magnetic field, Tellus 8-2, 252 (1956).

95) H. P. Utech, M. C. Flemings, Elimination of solute banding in indium antimonide crystals by growth in a magnetic field, J. Appl. Phys. 35, 2021 (1966).

96) F. H. Busse, R. M. Clever, Stability of convection rolls in the presence of a vertical magnetic field, Phys. Fluids 25, 931 (1982).

97) R. M. Clever, F. H. Busse, Nonlinear oscillatory convection in the presence of a vertical magnetic field, J. Fluid Mech. 201, 507 (1989).

98) S. Cioni, S. Chaumat, J. Sommeria, Effect of a vertical magnetic field on turbulent Rayleigh-Benard convection, Phys. Rev. E 62-4, 4520 (2000).

99) E. Guray, H. I. Tarman, Thermal convection in the presence of a vertical magnetic field, Acta Mech. 194, 33 (2007).

100) T. Alboussiere, D. Henry, S. Kaddeche, Note on braking and stabilization laws for buoyant fows under a weak magnetic field, Fluid Dyn. Res. 33, 287 (2003).

101) S. Kenjeres, K. Hanjalic, On the implementation of effects of Lorentz force in turbulence closure models, Int. J. Heat Fluid Flow 21, 329 (2000).

102) S. Kenjeres, J. Verdoold, M. J. Tummers, K. Hanjalic, C. R. Kleijn, Numerical and experimental study of electromagnetically driven vortical flows, Int. J. Heat Fluid Flow 30, 494 (2009).

103) G. M. Oreper, J. Szekely, The effect of an externally imposed magnetic field on buoyancy driven flow in a rectangular cavity, J. Cryst. Growth 64, 505 (1983).

104) M. Venkatachalappa, C. K. Subbaraya, Natural convection in a rectangular enclosure in the presence of a magnetic field with uniform heat flux from the side walls, Acta Mech. 96, 13 (1993).

105) N. Rudraiah, R. M. Barron, M. Venkatachalappa and C. K. Subbaraya, Effect of a magnetic field on free convection in a rectangular enclosure, Int. J. Eng. Sci. 33, 1075 (1995).

106) S. C. Kakarantzas, I. E. Sarris, N. S. Vlachos, Natural convection of liquid metal in a vertical annulus with lateral and volumetric heating in the presence of a horizontal magnetic field, Int. J. Heat Mass Transfer 54, 3347 (2011).

107) J. P. Garandet, T. Alboussiere, Bridgman growth: modelling and experiments, Prog. Cryst. Growth Charact. Mater. 38, 73 (1999).

108) A.Y. Gelfgat, P. Z. Bar-Yoseph, A. Solan Effect of axial magnetic field on threedimensional instability of natural convection in a vertical Bridgman growth configuration. J. Cryst. Growth 230, 63 (2001).

109) T. Munakata and I. Tanasawa, Onset of oscillatory flow in Czochralski growth melt and its suppression by the magnetic field, J. Cryst. Growth 106, 566 (1990).

110) K. Okada and H. Ozoe, Experimental Heat Transfer Rates of Natural Convection of Molten Gallium Suppressed Under an External Magnetic Field in Either the X, Y, or Z Direction, J. Heat Trans. 114, 107 (1992).

111) Y. C. Won, K. Kakimoto and H. Ozoe, Transient three-dimensional numerical computation for unsteady oxygen concentration in a silicon melt during a Czochralski process under a cusp-shaped magnetic field, J. Cryst. Growth 233, 622 (2001).

112) B. C. Sim, I. K. Lee, K. H. Kim and H. W. Lee, Oxygen concentration in the Czochralski-grown crystals with cusp-magnetic field, J. Cryst. Growth 275, 455 (2005).

113) M. Watanabe, M. Eguchi and T. Hibiy, Flow and temperature field in molten silicon during Czochralski crystal growth in a cusp magnetic field, J. Cryst. Growth 193, 402 (1998).

114) D. T. J. Hurle, Temperature oscillations in molten metals and their relationship to growth stria in melt grown crystals, Philos. Mag. 13, 305 (1966).

115) D. T. J. Hurle, E. Jakeman and C. P. Johnson, Convective temperature oscillations in molten gallium, J. Fluid Mech. 64, 565 (1974).

116) L. Davoust, M. D. Cowley, R. Moreau and R. Bolcato, Buoyancy-driven convection with a uniform magnetic field. Part 2. Experimental investigation, J. Fluid Mech. 400, 59 (1999).

117) J. M. Aurnouy, P. L. Olson, Experiments on Rayleigh-Benard convection, magnetoconvection and rotating magnetoconvection in liquid gallium, J. Fluid Mech. 430, 283 (2001).

118) U. Burr, U. Muller, Rayleigh-Benard convection in liquid metal layers under the influence of a horizontal magnetic field, J. Fluid Mech. 453, 345 (2002).

119) T. Yanagisawa, Y. Yamagishi, Y. Hamano, Y. Tasaka, and Y. Takeda, Spontaneous flow reversals in Rayleigh-Benard convection of a liquid metal, Phys. Rev. E 83, 036307 (2011).

120) B. Hof, A. Juel, T. Mullin, Magnetohydrodynamic damping of convective flows in molten gallium, J. Fluid Mech. 482, 163 (2003).

121) M. Kaneda, T. Tagawa, H. Ozoe, Natural convection of liquid metal under a uniform magnetic field with an electric current supplied from outside, Exp. Therm Fluid Sci. 30, 243 (2006).

122) B. Xu, B. Q. Li and D. E. Stock, An experimental study of thermally induced convection of molten gallium in magnetic fields, Int. J. Heat Mass Transf. 49, 2009 (2006).

123) M. Bonvalot, P. Courtois, P. Gillon and R. Tournier, Magnetic-levitation stabilized by eddy currents, J. Magn. Magn. Mater. 151, 283 (1995).

124) H. Yasuda, I. Ohnaka, Y. Ninomiya, R. Ishii, S. Fujita and K. Kishio, Levitation of metallic melt by using the simultaneous imposition of the alternating and the static magnetic fields, J. Cryst. Growth 260, 475 (2004).

125) T. Yanagisawa, Y. Yamagishi, and Y. Hamano, Detailed investigation of thermal convection in a liquid metal under a horizontal magnetic field: Suppression of oscillatory flow observed by velocity profiles, Phys. Rev. E 82, 056306 (2010).

126) O. Andreev and A. Thess., Visualization of magnetoconvection, Phys. Fluids 15, 3886 (2003).

127) G. S. Settles, Schlieren and shadowgraph techniques, Springer, Berlin, 2001.

128) W. M. Haynes, Handbook of chemistry and physics, CRC Press, Boca Raton, FL, 94th ed., 5-73 (2013).

129) P. Manneville, Rayleigh-Benard convection, thirty years of experimental, theoretical, and modeling work, Springer Tracts in Modern Physics 207, 41 (2006).

130) L. Rayleigh, On convection currents in a horizontal layer of fluid, when the higher temperature is on the under side. Phil. Mag. 32-6, 529 (1916).

131) J. A. Dean, Lange's handbook of chemistry, McGraw-Hill, New York, 13th ed., 6-38-43 (1985).

132) Den-netsu handbook (JSME Heat Transfer Handbook), Japan Society of Mechanical Engineering, Tokyo, 105(1993) [in Japanese].

ACHIEVEMENTS

Publications

1. **Yan Wang**, Noriyuki Hirota, Hidehiko Okada, Tie Liu, Qiang Wang, Yoshio Sakka, "*In-situ* observation of diamagnetic fluid flow in high magnetic fields", Key Engineering Materials, 616 188-193 (2014).

2. **Yan Wang**, Noriyuki Hirota, Hidehiko Okada, Yoshio Sakka, "Effects of high magnetic fields on thermal convection of conductive aqueous solution", Japanese Journal of Applied Physics, 54 077301 (2015).

3. **Yan Wang**, Noriyuki Hirota, Hidehiko Okada, Yoshio Sakka, "Effects of high magnetic fields on thermal convection using feeble magnetic conductive aqueous solutions", Bulletin of the Chemical Society of Japan, in press.

Conferences/ Symposiums

Oral/Poster Presentations

1. **Yan Wang**, Noriyuki Hirota, Hidehiko Okada, Tie Liu, Qiang Wang, Yoshio Sakka, "*In-situ* observation of diamagnetic fluid flow in high magnetic fields", Joint Conference of The 5th International Symposium on Advanced Ceramics (ISAC-5) hold in conjunction with The 3rd International Symposium on Advanced Synthesis and Processing Technology for Materials (ASPT2013), Wuhan, 9th-12th December 2013 – **Oral presentation.**

2. **Yan Wang**, Noriyuki Hirota, Hidehiko Okada, Tie Liu, Qiang Wang, Yoshio Sakka, "*In-situ* observation of diamagnetic fluid flow in high magnetic fields", 6th International Workshop on Materials Analysis and Processing in Magnetic Fields, Okinawa, Japan, 8th-11th July 2014 – **Poster presentation**.